

Characterizing the Impacts of Shale Barriers and Lean Zones on SAGD Performance
with Data-Driven Modeling Techniques

by

Cui Wang

A thesis submitted in partial fulfillment of the requirements for the degree of

Master of Science

in

Petroleum Engineering

Department of Civil and Environmental Engineering
University of Alberta

© Cui Wang, 2015

Abstract

Performance of steam-assisted gravity drainage (SAGD) is influenced significantly by the distributions of shale barriers and lean zones, which tend to impede the vertical growth and lateral spread of a steam chamber. Reliable appraisal and prediction of SAGD require a comprehensive understanding of the effects of shale barriers and lean zones on SAGD performance. However, a comprehensive and systematic investigation of the heterogeneous distribution (location, continuity, size, proportion and saturation) of shale barriers and lean zones is still lacking.

In this study, numerical simulations are used to model the SAGD process. First, a detailed sensitivity analysis is performed by varying the location, continuity, size, proportion, and saturation of these heterogeneous features. Shale barriers (imbedded in a region of degraded rock properties) and lean zones with different sizes and degrees of continuity are placed in areas above the injector, below the producer, or in between the well pair. Then, the distribution of shale barriers and lean zones is stochastically modeled by nested sequential indicator simulation. A set of attributes, such as facie proportions and dimensionless correlation lengths, which represent the characteristics of reservoir heterogeneities are identified on the basis of the knowledge learned from preceding sensitivity analysis. Finally, neural network modeling is used for constructing data-driven models to correlate the pertinent attributes to SAGD performance measures.

This work provides a guideline for assessing the impacts of shale barrier and lean zone heterogeneities on SAGD performance. A set of input variables and parameters that

have significant impacts on the ensuing recovery response is identified. One can define readily the proposed set of variables from well logs and apply immediately in data-driven models with field data and scale-up analysis of experimental models to assist field-operation design and evaluation. One can also extend the approach presented in this thesis to analyze other solvent-assisted SAGD processes.

Acknowledgments

I would like to express my sincerest love to my family, my parents, my brother, for their unflagging support and endless love, throughout my studies.

I am very thankful to my supervisor, Dr. Juliana Leung, for having faith on me, for giving me an opportunity to work on this project, for all of her encouragement and support. I would like to thank Dr. Ergun Kuru and Dr. Huazhou Li, my examining committee members.

I gratefully acknowledge the financial support from Natural Sciences and Engineering Council of Canada (NSERC) for this research through grants held by Dr. Juliana Leung. I am also thankful to Computer Modeling Group Ltd. (CMG) for providing the CMG software package for the simulation study.

I am thankful to Siavash Nejadi, Zhiwei Ma, Mingyuan Wang, Vishal Vikrant, and Ehsan Amirian for their valuable guidance and suggestions that are helpful in improving my reservoir engineering skills. Finally, I would like to thank all those who helped and inspired with me throughout my research.

Table of Contents

Abstract.....	II
Acknowledgments	IV
Table of Contents	V
List of Tables.....	VII
List of Figures.....	VIII
Chapter 1: General Introduction.....	1
1.1 Problem Statement	1
1.2 Research Objectives	3
1.3 Thesis Layout.....	4
Chapter 2: Literature Survey	5
2.1 SAGD Process	5
2.2 Review of SAGD Investigation.....	6
2.3 Artificial Neural Network.....	13
Chapter 3: Research Methodology	16
3.1 Reservoir Property Modeling.....	16
3.1.1 Reservoir Model Description	16
3.1.2 Multiphase Flow Functions.....	17
3.2 Heterogeneity Modeling.....	18
3.2.1 Facie and Rock Property Modeling	18
3.2.2 Procedure of Generation of Multiple Stochastic Realizations	21
3.3 Performance Ranking	21
3.4 Artificial Neural Network for Data-Driven Model.....	22
3.5 Principle Component Analysis	24

3.6 Sensitivity Analysis of Grid Size	25
Chapter 4: Assessing Impacts of Reservoir Heterogeneities on SAGD Performance	
.....	35
4.1 Effects of Lean Zones on SAGD Performance	35
4.1.1 Top Water	35
4.1.2 Bottom Water	37
4.2 Effects of Shale Distribution on SAGD Performance	39
4.2.1 Continuous Shale Barrier	40
4.2.2 Discontinuous Shale Barrier	43
Chapter 5: Correlation of Reservoir Heterogeneities to SAGD Performance Using	
Data-Driven Modeling Methods	53
5.1 Correlation of Heterogeneity Attributes to SAGD Performance Indicators ...	53
5.2 Stochastic Distribution of Shale Barrier and Lean Zone	57
5.3 Derivation and Calculation of Reservoir Heterogeneities Parameters	62
Chapter 6: Conclusion	71
Nomenclature	75
References	80
Appendix A: Combination of Facy Maps and Property Maps	89
Appendix B: Calculation of DB	105

List of Tables

Table 3-1 Parameters in Eqn. (3-1)	27
Table 3-2 Reservoir and Fluid Properties	27
Table 3-3 Parameters in Archie Equation	27
Table 4-1 Simulation Results for Cases with Top Water	46
Table 4-2 Simulation Results for Cases with Bottom Water.....	46
Table 4-3 Simulation Results for Single Continuous Shale Barrier without LQS.....	47
Table 4-4 Simulation Results for Single Continuous and Discontinuous Shale Barrier with LQS	47
Table 4-5 Simulation Results for Randomly-Distributed Discontinuous Shale Barriers with LQS with Fixed Shale Barrier Thickness	48
Table 4-6 Simulation Results for Randomly-Distributed Discontinuous Shale Barriers with LQS with Fixed Shale Barrier Length	48
Table 5-1 Range of Dimensionless Input Attributes for ANN Modeling	64
Table 5-2 Range of Dimensionless Input Attributes for ANN Modeling (Stochastic)	64
Table 5-3 Correlation Coefficients for ANN Modeling (Stochastic).....	64

List of Figures

Figure 2-1 An ANN is an interconnected group of nodes. The circle represents an artificial neuron, and the arrow represents a connection between two neurons.	15
Figure 3-1(a) Configuration and setup for 2D (X-Z plane) SAGD simulation.	28
Figure 3-1(b) Schematic of steam chamber expansion in a SAGD displacement.	28
Figure 3-2 Oil viscosity profile as a function of temperature.	29
Figure 3-3(a) Relative permeability functions in clean sand and LQS for water-oil system.	29
Figure 3-3(b) Relative permeability functions in clean sand and LQS for liquid-gas system.	30
Figure 3-4(a) Relative permeability functions in shale barrier for water-oil system.	30
Figure 3-4(b) Relative permeability functions in shale barrier for liquid-gas system.	31
Figure 3-5 Capillary pressure functions for water-oil system in shale barrier.	31
Figure 3-6 Capillary pressure functions for liquid-gas system in shale barrier.	32
Figure 3-7(a) Histogram of porosity for clean sand by use of SGSIM.	32
Figure 3-7(b) Histogram of porosity for LQS by use of SGSIM.	33
Figure 3-7(c) Histogram of porosity for shale barrier by use of SGSIM.	33
Figure 3-7(d) Variogram of porosity distribution for clean sand, LQS, and shale barrier by use of SGSIM.	34
Figure 3-8 Distribution for clean sand, LQS and shale barriers, and corresponding porosity, water saturation distribution.	34
Figure 4-1 Oil saturation distribution after 2 years for varying top water thickness.	49
Figure 4-2 Oil saturation distribution after 5 years for varying bottom water thickness.	49
Figure 4-3 Permeability distribution (in darcies) for various shale distributions.	50
Figure 4-4 Impacts of capillarity on oil rate and iSOR over 20 years for a single	

continuous shale barrier located at $z = 10$	50
Figure 4-5 Comparison of RF and CSOR for 20 years for single continuous shale barrier at $z = 10$ with and without LQS.	51
Figure 4-6 Oil saturation distribution after 5 years for different locations (z) of the single continuous shale barrier with LQS.	51
Figure 4-7 RF and CSOR for 20 years with different locations (z) of the single continuous shale barrier with LQS.	52
Figure 4-8 Oil saturation distribution after 5 years for different l_{Dsh} for randomly-distributed discontinuous shale barriers with LQS.	52
Figure 5-1 Cross plot of actual flow simulation results (target values) of normalized R against network predictions: training data set (left) and testing data set (right).	65
Figure 5-2 Cross plot of actual flow simulation results (target values) of normalized DB against network predictions: training data set (left) and testing data set (right).	65
Figure 5-3 Temperature distribution after 10 years SAGD simulation for: Left: stochastic lean zone, and Right: constant water saturation of 0.0667.	65
Figure 5-4 Schematic illustrating the stochastic distribution of shale and LQS.....	66
Figure 5-5 Cross plot of actual flow simulation results (target values) of normalized R against network predictions using all 9 original input attributes: training data set (left) and testing data set (right).	66
Figure 5-6 Cross plot of actual flow simulation results (target values) of normalized DB against network predictions using all 9 original input attributes: training data set (left) and testing data set (right).	67
Figure 5-7 Cross plot of actual flow simulation results (target values) of normalized t_{DISOR} against network predictions using all 9 original input attributes: training data set (left) and testing data set (right).....	67

Figure 5-8 Cross plot of actual flow simulation results (target values) of normalized R against network predictions using 5 principal scores as input attributes: training data set (left) and testing data set (right). 67

Figure 5-9 Cross plot of actual flow simulation results (target values) of normalized DB against network predictions using 5 principal scores as input attributes: training data set (left) and testing data set (right). 68

Figure 5-10 Cross plot of actual flow simulation results (target values) of normalized t_{DISOR} against network predictions using 5 principal scores as input attributes: training data set (left) and testing data set (right). 68

Figure 5-11 Cross plot of actual flow simulation results (target values) of normalized R against network predictions for the case in which lateral heterogeneities are ignored and all 9 original input attributes are used: training data set (left) and testing data set (right). 68

Figure 5-12 Cross plot of actual flow simulation results (target values) of normalized DB against network predictions for the case in which lateral heterogeneities are ignored and all 9 original input attributes are used: training data set (left) and testing data set (right). 69

Figure 5-13 Cross plot of actual flow simulation results (target values) of normalized t_{DISOR} against network predictions for the case in which lateral heterogeneities are ignored and all 9 original input attributes are used: training data set (left) and testing data set (right). 69

Figure 5-14 Cross plot of actual flow simulation results (target values) of normalized R against network predictions for the case in which lateral heterogeneities are ignored and 5 principal scores are considered as input attributes: training data set (left) and testing data set (right). 69

Figure 5-15 Cross plot of actual flow simulation results (target values) of normalized DB against network predictions for the case in which lateral heterogeneities are

ignored and 5 principal scores are considered as input attributes: training data set (left) and testing data set (right)..... 70

Figure 5-16 Cross plot of actual flow simulation results (target values) of normalized t_{DISOR} against network predictions for the case in which lateral heterogeneities are ignored and 5 principal scores are considered as input attributes: training data set (left) and testing data set (right). 70

Chapter 1: General Introduction

In this chapter, the problems motivating this research are first presented. Then, the objectives of this research are listed. Finally, the layout of this research is presented to introduce this study briefly.

1.1 Problem Statement

Performance of SAGD is influenced significantly by the distributions of lean zones and shale barriers, which tend to impede the vertical growth and lateral spread of a steam chamber. Reliable appraisal and prediction of SAGD require a comprehensive understanding of the effects of reservoir heterogeneities on SAGD performance.

Real reservoir typically consists of complex facies, where shale sand is stochastically distributed but separated with clean sand by a natural low-quality-sand (LQS) transition zone. However, in the literature survey, few researches considered the existence of LQS typically surrounding the shale layers, because the shale has a more significant effect on the spatial expansion of steam chamber. In addition, variability in multiphase-flow functions (capillary pressure and relative permeability) of different rock facies is often ignored in previous studies by assigning identical capillary pressure and relative permeability relationships to both sands and shales. Because many classical works have already demonstrated the strong influences of lithological characteristics and pore geometry on multiphase-flow functions (Botset 1940; Morgan and Gordon 1970), one should consider appropriate relative permeability and capillary pressure models for

different rock types when analyzing the effects of reservoir heterogeneities on SAGD performance.

Also, most prior investigation limited the lean zones as top water or bottom water, but water can stochastically exist in reservoir based on the well log information. Although previous works have partially provided many useful insights regarding the modeling of shale barriers/lean zones and their impacts on short-/long-term recovery performance, a comprehensive and systematic investigation of the heterogeneous distribution (location, continuity, size, proportion and saturation) of shale barriers and lean zones is still lacking.

Laboratory-scale experiments and reservoir simulations are two typical methods to study impacts of reservoir heterogeneity on SAGD process. In experimental analysis, the difficulty is the modeling of stochastic distribution of shale barriers/lean zones. Reservoir simulation is typically time consuming and invokes many assumptions, especially for field-scale simulation, and not suitable for real-time decision making or forecasting, though it is useful for detailed study of displacement process. This motivates an alternative approach of SAGD performance prediction based on data-driven models. However, a set of input attributes suitable for characterizing the heterogeneities of shale layers and lean zones in SAGD reservoirs is not readily identifiable from existing literature. A more fundamental description and understanding of the effects of heterogeneities on recovery performance is in demand. This understanding would also become the basis for formulating numerous input attributes in subsequent data-driven modeling: artificial neural networks (ANN) or fuzzy-based models can be used to

construct data-driven models that relate input (predicting) attributes describing reservoir/fluid/operational variables to output (target) attributes representing recovery performance.

1.2 Research Objectives

The objective of this study is to study the effects of reservoir heterogeneities on SAGD performance by numerical simulation:

- (1) A comprehensive and systematic investigation of the heterogeneous distribution (location, continuity, size, proportion, and saturation) of shale barriers and lean zones will be presented. Multiple facies in reservoir, including a gradation of properties exists between shale barrier and clean sand, will be considered. Appropriate relative permeability and capillary pressure models for different rock types will be considered.
- (2) Reservoir heterogeneities will be modeled by stochastic distribution of shale barriers and lean zones to mimic the practical scenario.
- (3) ANN will be used to construct data-driven models that relate input attributes describing reservoir variables to output (target) attributes representing recovery performance. Therefore, a set of parameters suitable for characterizing the heterogeneities of shale barriers and lean zones in SAGD reservoirs should be identified and can be applied immediately in data-driven models with field data to assist field-operation design and evaluation.

1.3 Thesis Layout

In the next chapter, the process of SAGD is summarized and previous studies related to the impacts of reservoir heterogeneities on SAGD performance are reviewed. A detailed literature review on the application of ANN in petroleum engineering is also included in the next chapter. Chapter 3 presents the methodology employed in this study. Details of the model set-up and numerical simulation are discussed. The techniques of sequential indicator simulation and sequential Gaussian simulation are introduced to model stochastic distribution of shale barriers. Chapter 4 presents a comprehensive sensitivity analysis of the effects of shale and lean zone distribution on SAGD performance, including location, continuity, size, proportion and saturation. A set of input variables for correlating relevant parameters to ranking results are identified. Chapter 5 investigates the application of ANN for correlating the parameters identified in Chapter 4 to SAGD performance measures. The principal component analysis (PCA) method is used here to reduce the dimensionality of the input variables. Chapter 6 summarizes the major findings of the conducted research and presents suggestions for future research.

Chapter 2: Literature Survey

In this chapter, literature survey helps understand what has been done in the past on the topic of this research. Improvement of this research compared to previous study is then highlighted. The research focuses on the effects of reservoir heterogeneities on SAGD process, so this chapter starts with a brief introduction of SAGD process.

2.1 SAGD Process

The huge quantity (approximately 7 trillion bbl) of heavy oil/bitumen discovered worldwide shows its increasing economic potential, especially when conventional oil production continuously declines (Albahlani and Babadagli 2008). Canada and Venezuela have the greatest amounts (1.7 trillion bbl and 1.8 trillion bbl, respectively) of bitumen and heavy oil reserves (Burton et al. 2005, Nasr and Ayodele 2006). More than 60% of the total natural bitumen resources are in the province of Alberta (Attanasi and Meyer, 2007).

Extremely high viscosity of the heavy oil/bitumen at reservoir temperature, however, is one of the significant challenges for the recovery process (Chen et al. 2008; Dang et al. 2010). Because of its high viscosity, conventional non-thermal technology cannot produce the oil efficiently and economically. Instead, success with several thermal methods, such as steam injection and electromagnetic heating, was demonstrated. Among the thermal processes, steam assisted gravity drainage (SAGD), which was pioneered and developed by Butler (Butler and McNab, 1981), is the most widely adopted technology

for commercial production in Alberta (Ipek et al. 2008).

SAGD is an enhanced oil recovery technology by which steam is injected into the reservoir with a horizontal well pair spaced 5 to 10 m from each other, with the injector at the top and the producer at the bottom. The injected steam creates a high temperature chamber, in which the viscosity of heavy oil is dramatically decreased, and the oil drains along the walls of the chamber toward the producer caused by gravitational forces (Hampton et al. 2013). With gravity drainage as the primary mechanism, SAGD can avoid the potential challenges of steam override (Chen 2009). In addition, the viscosity of the heated oil remains low, whereas in other conventional steam-flooding methods, oil viscosity increases as it cools and flows to the production well (Chen et al. 2008).

2.2 Review of SAGD Investigation

Because of the importance of SAGD, understanding the complex physics of SAGD is essential so that reliable prediction and effective design can be made. Richardson et al. (1978) developed a mathematical model to study the effects of shale barrier on SAGD performance. They found that the size and distribution of shale barriers played an essential role on SAGD production. Also, they presented that computer blocks with a reduced vertical permeability can mimic the effects of shale barrier, which gave evidence for simulation study of SAGD process with more complex physics. Theory of SAGD process has been presented by assuming homogeneous and isotropic reservoir (Butler and McNab 1981, Butler 1985). Butler (1985) developed a semi-analytical model to calculate

the oil drainage rate, heat penetration rate, and the “S-shaped” interface advancement with homogenous and isotropic reservoir properties.

After Butler’s study, various investigation modified and improved Butler’s gravity-drainage model, which made the model more realistic for industry. A model with linear steam chamber was developed by Reis (1992). A modified approach for calculating the local velocity and temperature distribution was proposed to better match the experimental data. Other researchers have proposed semi-analytical models, in which analytical solutions of the momentum and mass balances performed at the solvent-oil interface are incorporated into a calculation sequence to advance the steam chamber interface and to compute oil recovery. These models were applied successfully to provide approximate solutions for 2D cross-sectional realizations (Vanegas et al. 2008; Azad and Chalaturnyk, 2010).

A major shortcoming of analysis with analytical models lies in their limited capabilities for incorporating reservoir heterogeneities, rendering them rather deficient in studying the impacts of features such as shale barriers and lean zones. For example, less permeable shale barriers can hamper vertical propagation of the steam chamber, whereas lean zones with low oil saturation increases heat loss. Simplified physics and assumptions invoked in nearly all analytical or semi-analytical models cannot fully capture these complex heterogeneities.

The impacts of the reservoir heterogeneity on the SAGD process were assessed in the past with different approaches: laboratory-scale experiments and reservoir simulations.

In the experiments by Joshi and Threlkeld (1985), a box-shaped sand pack was filled with 20-30 mesh (0.84-0.58 mm diameter) Ottawa sand for heavy oil displacements. Shale barriers were simulated by installing 6 mm thick plastic sheets. They observed that the final SAGD oil recovery at a fixed time was reduced when shale barriers were added in the sand pack. In addition, initial oil production rate was faster in the presence of shale barrier because the shale could divert the injected steam to the reservoir portion above it and accelerate oil production. Yang and Butler (1992) performed a series of 2-D SAGD experiments using porous media (0.21 m in height) consisting of 2-mm and 3-mm glass beads, with shale barriers of varying continuity (length) placed above the injector. A sealed, 0.4 cm thick, reinforced, phenolic resin divider was inserted to model the thin shale layer. They found that short horizontal barriers did not have considerable effects on SAGD performance, whereas the longer horizontal barriers would decrease the production rate significantly. Law et al. (2003) used an elemental approach to investigate the effects of top thief (lean) zone on drainage rate and steam loss. The 60 cm × 30 cm diameter high-pressure vessel was constructed to mimic the cylindrical physical model.

A primary challenge with experimental analysis is that laboratory studies are typically time-consuming, whereas operation conditions, such as injection rate, are difficult to control in heterogeneous models. Although lab-scale measurements are available at a length scale ≤ 1 m, extrapolating these fine-scale measurements to field-scale values, where heterogeneity correlates over a much larger distance, remains difficult.

Those difficulties with experimental analysis can be partially overcome with numerical simulation, which was widely used to monitor the advancement of steam chambers (Lerat et al. 2010; Leskiw and Gates 2012), and to optimize operational strategies (Zhao et al. 2007, Mohebati et al. 2010, Nguyen et al. 2012) and to investigate the effects of reservoir heterogeneities on SAGD performance (Pooladi-Darvish and Mattar 2002; Ipek et al. 2008; Hampton et al. 2013; Wang and Leung 2015).

Pooladi-Darvish and Mattar (2002) constructed a series of 2D layered models on the basis of underground test facility (UTF) field data to study the effects of shale continuity in the vertical direction on SAGD operations in the presence of gas cap and top water. Four different permeable levels were tested to represent the scenarios of sealing shale, partially sealing shale, homogeneous formation, and communicating shale. In each case, an effective permeability at the modeling scale of 1 m was obtained with a power average as a function of shale volume. The authors observed only a minor effect on the SAGD performance. In addition, the permeability averaging might have masked and smeared the effects of shale barrier connectivity on the resultant production behavior.

Ipek et al. (2008) incorporated the effects of geomechanics in SAGD operations for a series of reservoirs with varying degrees of shale content. They investigated the potential of pressure cycling as a method of enhancing reservoir permeability to offset the negative effects of shale barriers. Chen et al. (2008) studied the effects of shale barriers on SAGD performance with a series of 2-D geostatistical models in which shale layers, characterized by low vertical permeability (typically in the range of 10^{-6} to 10^{-3} mD), are

distributed stochastically in the near-well region (NWR) and the above-well region (AWR). The authors assumed that the laterally oriented thin shale lenses would have no impact on the horizontal permeability. A sensitivity analysis was performed by varying the correlation length and proportions of the shale. It was observed that shale layers hindered the fluid drainage within the NWR and the expansion of the steam chamber in the AWR. Their results also confirmed that SAGD performance was affected adversely only when the AWR contains long, continuous shale, an observation that was consistent with the findings of Yang and Butler (1992).

Hampton et al. (2013) studied the effects of thermal conductivity and permeability heterogeneity (introduced by the presence of shale lenses) on SAGD performance. Geostatistical realizations of shale distributions with varying correlation length were modeled, and it was concluded that variations in permeability affected the steam chamber development more prominently than variations in thermal conductivity. One should note that not one of these works has considered the effects of capillary pressure in shale.

Another origin of reservoir heterogeneity stems from spatially-varying water distribution. Highly-permeable lean zones could promote lateral spreading of the steam chamber. Lean zones could act as thief zones causing severe heat loss during the SAGD process (Xu et al. 2014a, Wang and Leung 2015). Law et al. (2003) investigated the field-scale SAGD performance in the presence of confined and unconfined top water. A baseline run was performed first with no top water zone in the SAGD process. Effects of the top water zone and optimization of operation conditions in the presence of top water

zone were analyzed by comparison with the base case. Effects of injection pressure and initial pressure in the top water zone were investigated. Their results suggest that increasing the pressure difference between the steam chamber and the top water zone would lead to unfavorable SAGD performance.

In reservoirs with underlying bottom water (Masih et al. 2012), the performance of SAGD depends on the vertical offset and pressure differential between the producer and the water zone. Ricardo (2013) confirmed through numerical simulations that the negative impacts of bottom water increases with its thickness; a vertical offset of 5 m was determined to be the optimum in terms of project economics. Results of these studies highlighted the adverse impacts on SAGD efficiency due to heat loss through these heterogeneous features/thief zones. However, detailed description of the impacts of randomly-distributed water saturation (as often inferred from well log measurements) is lacking. Xu et al. (2014b) presented a hybrid CSS/SAGD design study using a stochastic lithological model constructed via sequential Gaussian simulation; the water saturation was assigned deterministically subject to the facie distribution.

Although numerical simulation can provide detailed study of displacement process, it is typically time consuming and invokes many assumptions, especially for field-scale simulation in which millions of gridblocks are required. Thus, the alternative approaches of SAGD performance prediction based on data-driven models were applied. Weiss et al. (2002) used artificial intelligence tools such as fuzzy logic and neural networks to forecast oil production based on historical information. Their results showed that an

estimate of oil production rate in the first year could be obtained if well logs information were given. The error between prediction and target could be minimized if a large datum was available. Amirian et al. (2013) used a series of attributes that described reservoir heterogeneities as inputs for their artificial neural network (ANN) model. Their results exhibited good correlation and prediction between the given inputs and the outputs associated with the SAGD performance. Ma et al. (2015) analyzed the exploratory data and extracted inputs describing reservoir heterogeneity and operation conditions for their ANN model. They confirmed that ANN could be implemented in a practical manner for SAGD performance prediction. Therefore, the next section in this chapter is to introduce the background of ANN which is used in this research.

In the aforementioned studies, shale barriers are represented by a series of low-permeability layers distributed either stochastically or uniformly in the background domain composed of clean sand. However, a gradation of properties exists between the shale barriers and background clean sands, particularly in the inclined heterolithic strata deposits. Hubbard et al. (2011) observed four different lithofacies, involving coarse grains, fine- to medium-grain, interbedded fine-grain, and thin very-fine-grain, from the seismically-imaged depositional elements. Smith et al. (2009) also reported varying grain size distributions in counter point bar deposits in McMurray formations.

In addition, variability in multiphase flow functions (capillary pressure and relative permeability) of different rock facies is often ignored in previous studies by assigning identical capillary pressure and relative permeability relationships to both sands and

shales. Because that many classical works have already demonstrated the strong influences of lithological characteristics and pore geometry on multiphase flow functions (Botset 1940; Morgan and Gordon 1970), one should consider appropriate relative permeability and capillary pressure models for different rock types when analyzing the effects of reservoir heterogeneities on SAGD performance.

Finally, the previous studies have provided many useful insights regarding the modeling of shale barriers/lean zones and their impacts on short-/long-term recovery performance; however, analysis that aims to correlate a set of input parameters descriptive of reservoir heterogeneity introduced by shale barriers and lean zones to SAGD production performance is unavailable. The ability to formulate such parameters from well log or other petrophysical data would facilitate the construction of data-driven or statistical models for SAGD production analysis.

2.3 Artificial Neural Network

The artificial neural network (ANN) is a virtual-intelligence method used to approximate a nonlinear relationship between input and target variables. Initially, ANN is inspired based on human's central nervous systems that are capable of machine learning and pattern recognition. ANN is developed by training the network to represent the intrinsic relationships existing within the data. This idea was created by neurophysiologist Warren McCulloch and mathematician Walter Pitts (McCulloch and Pitts 1943). They modeled a simple neural network by use of electrical circuits to explain how neurons function in the

brain. In the past decades, combination of many neurons in neural networks can be more promising than single neurons.

A schematic of various elements of an ANN consisting of only one hidden layer is illustrated in **Fig. 2-1**. A series of neurons are assigned in the hidden layers, in which nonlinear activation functions are applied to the weighted summation of input signals. Weights and biases associated with each connection in the network are determined by means of a supervised learning process, by which the mismatch between network predictions and known values of the target variables is minimized with a set of training data consisting of known input and output attributes (Francis 2001).

ANN is widely applied in petroleum engineering (Mohaghegh 2002, Bravo et al. 2012), such as reservoir property prediction, history matching and design of well trajectory. Recently, neural network has been used as a proxy model to predict oil recovery (Queipo et al. 2002, Ahmadloo et al. 2010).

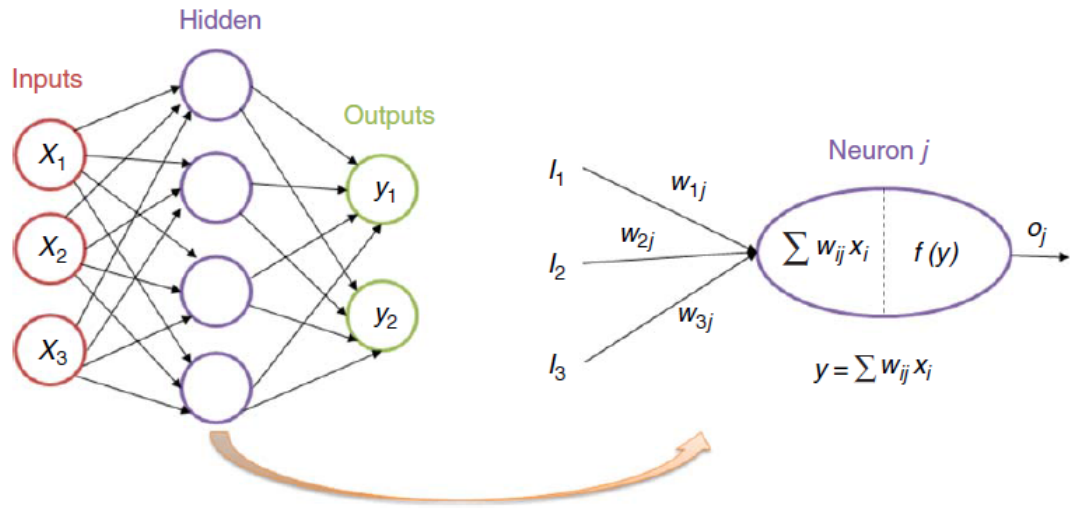


Figure 2-1 An ANN is an interconnected group of nodes. The circle represents an artificial neuron, and the arrow represents a connection between two neurons.

Chapter 3: Research Methodology

In this chapter, reservoir and fluid models are presented in detail, which will be used in the subsequent simulations. Then, the detailed procedure of modeling of stochastic distribution of shale barriers and lean zones is presented. The tool of artificial neural network to analyze the simulation results will also be discussed in this chapter.

3.1 Reservoir Property Modeling

3.1.1 Reservoir Model Description

A commercial thermal-compositional simulator (Computer Modelling Group 2013) is used to construct a 2D (x-z) numerical model representative of a typical Athabasca oil-sand reservoir. As shown in **Fig. 3-1 (a)**, the reservoir is 200-m deep with a pay zone of 30 m in thickness. The model is 51 and 30 m in the x- and z- direction, respectively, with $\Delta x = \Delta y = 1$ m. A lateral leg of 900 m is oriented along the y-direction. The producer is at $z=26$, which is 5 m below the injector at $z=21$. The locations of the well pair are also shown in Fig. 3-1 (a). The model setup exemplifies a confined drainage pattern, similar to many previous works such as Chen et al. (2008), where only one-half of a steam chamber is simulated. A schematic illustrating the steam chamber expansion is shown in **Fig. 3-1 (b)**. In this model, only half of the well bore of injector and producer is used for injection and production, respectively. **Fig. 3-2** shows the oil-viscosity profile with temperature. The viscosity of the in-situ oil is 600,000 cp at the initial reservoir temperature of 18°C. As shown in the figure, the rate of oil viscosity decrease

becomes smaller as temperature increases. When the temperature is higher than 300°C, the oil viscosity is nearly constant. For all simulations, 100% quality steam is injected at 1900 kPa continuously for a total simulation time (t_s) of 20 years. A pre-heating period of 3 months is modeled to alleviate injectivity issues caused by unfavorable mobility ratio.

3.1.2 Multiphase Flow Functions

In this research, three different rock facies are modeled: clean sand, shale barrier, and low-quality sand (LQS) that exists as a transition zone between the clean sand and the shale barrier. Relative permeability relationships of oil/water and gas/liquid systems for the clean sand and LQS are adopted from Mohebati et al. (2010), as shown in **Fig. 3-3**. As for the shale facies, relative permeability is assigned in accordance with the experimental observations by Morgan and Gordon (1970), which show a narrower two-phase region and lower end-points in the shale. The modified shale relative permeability functions are shown in **Fig. 3-4**. Similar phase relative permeability functions were also used in Chen et al. (2008), although capillary pressure was ignored.

Similar to previous SAGD simulation studies, capillary pressure in the clean sand and LQS is assumed to be negligible, considering that the average grain size is sufficiently large. However, a similar assumption would not be valid in the shale. In this work, the capillary pressure function is formulated after Skjaeveland et al. (2000), which was based on the experimental evidence in Morrow and Harris (1965). Skjaeveland et al. (2000) adopted the following correlation for the water/oil system:

$$P_c = \frac{c_w}{\left(\frac{S_w - S_{wr}}{1 - S_{wr}}\right)^{a_w}} + \frac{c_o}{\left(\frac{S_o - S_{or}}{1 - S_{or}}\right)^{a_o}} \quad (3-1)$$

In **Eq. 3-1**, the parameters c_w , c_o , a_w and a_o , are empirical constants (**Table 3-1**). The S_w and S_o are the saturation for water and oil phases. $S_{wr}(0.15)$ and $S_{or}(0.2)$ refer to the residual saturation of oil and water phases, respectively. Considering the difference in the interfacial tension between the water/oil and the liquid/gas systems, Wang et al. (2006) proposed a multiplication factor to relate the capillary pressures of water/air and water/oil systems on the basis of experimental measurements. Although Wang et al. (2006) did not study two-phase displacements in SAGD, a similar factor of 3.0 is adopted to quantitatively characterize the difference of capillary pressure in two different systems. **Figs. 3-5 and 3-6** shows the capillary pressure functions for water/oil and liquid/gas in the shale, respectively.

3.2 Heterogeneity Modeling

3.2.1 Facie and Rock Property Modeling

As mentioned in Chapter 2, shale barriers and lean zones are distributed stochastically in practical field. Reliable prediction of SAGD performance requires realistic and accurate modeling of stochastic distribution of shale barriers and lean zones. In this section, shale barriers and lean zones are modeled stochastically by use of sequential indicator simulation (SISIM) and sequential Gaussian simulation (SGSIM) techniques.

Nested sequential indicator simulation (Deutsch 2002) is applied to stochastically model shale barriers, which are imbedded in a region of LQS, among a background of

clean sand. Within each facie, porosity values are populated using sequential Gaussian simulation (Deutsch and Journel 1998). LQS properties are modeled to depict a continuous gradation between shale barrier and clean sand. **Figs. 3-7 (a), (b), (c) and (d)** show the histograms and variogram to model the porosity distribution for different facies by use of SGSIM. As shown in Fig. 3-7, the mean values of porosity for clean sand, LQS and shale are 0.30, 0.18, and 0.05, respectively. For the variogram plot, the γ is calculated by the following equation:

$$\gamma(h) = \frac{\sum[\phi(x) - \phi(x+h)]^2}{2N_h} \quad (3-2)$$

Where, γ refers to semivariance, $\phi(x)$ means the value of property (i.e. porosity) at location x , N_h is the number of data pairs separated by the distance h . In the variogram plot, the solid lines are the analytical solution of the semivariance along vertical and horizontal directions, while the dashed lines are the corresponding results for experimental data. The experimental semivariances are similar to the analytical solutions, which indicates that experimental data for porosity within each facie is reliable.

Chen et al. (2008) assumed that the presence of shale in sand reduces the vertical permeability dramatically but has no effect on the horizontal permeability. Following their suggestion, a constant horizontal permeability of 5 darcies is applied to all three facies in this study, and a factor of 10^{-8} to 10^{-4} and 0.2 to 0.8 is applied to the k_v/k_h in shale barriers and clean sand, respectively, which are similar to the values provided in Chen et al. (2008) and Dang et al. (2010). The continuous variation in k_v/k_h within each facie is also modeled by sequential Gaussian simulation. The variation in k_v/k_h ratio in the

LQS is modeled as the arithmetic average between the clean sand and shale barrier.

The same value of thermal conductivity is assigned for all three rock types, as suggested by Hampton et al. (2013). However, as shown in the paper by Yang and Butler (1992), the fluids have different thermal conductivity. Water phase has a higher thermal conductivity than oil and gas phases. The thermal conductivity of the gas phase is the smallest. The conductivity values of rocks and fluids and other reservoir properties are shown in **Table 3-2**. These parameters are comparable to those in the experimental studies by Yang and Butler (1992) and simulation studies of Chen et al. (2008).

Archie model (1942) is used to model the stochastic distribution of lean zones within the reservoir as a function of local porosity and formation resistivity:

$$S_w = ((aR_w)/(\phi^m R_t))^{1/n} \quad (3-3)$$

Where, a , m = cementation factor; n = saturation exponent; ϕ = porosity in fraction; R_t = true or formation resistivity, and R_w = water resistivity. McCoy and Grieves (1997) demonstrated that values of a and m do not vary significantly for different facies; however, n is observed to be the highest for clean sand and lowest for shale barrier. The values of R_w and R_t can be derived from the well log measurements. Values of these parameters, as summarized in **Table 3-3**, are assigned based on the representative trends for different rock groups presented in Palacky (1987). The formation resistivity is assumed to be constant within the facie. An example of facie, porosity and saturation distributions is shown in **Fig. 3-8**.

3.2.2 Procedure of Generation of Multiple Stochastic Realizations

The preceding subsection introduces the basic principles to model stochastic distribution of shale barriers and lean zones within reservoir. In this subsection, those basic principles are applied for generation of multiple realizations and are presented step by step. The number of multiple realizations is N_r here.

1. Generation of porosity and k_v/k_h distribution for clean sand, LQS, and shale barrier, respectively, by use of SGSIM;
2. Generation of N_r maps for clean sand and shaly sand, and N_r maps for LQS and shale barrier by use of SISIM. Note that shaly sand here consists of LQS and shale barrier. Superposition of the N_r shaly maps and the N_r shale maps can generate N_r maps consisting of clean sand, LQS and shale barrier;
3. Set up the facy properties by combining the facy maps (i.e. item 2) and property maps (i.e. item 1). This step is implemented by the Matlab code in **Appendix A**;
4. Calculation of water saturation by Eq. (3-3).

3.3 Performance Ranking

To facilitate the comparison between various cases, three ranking schemes (R, DB and t_{DISOR}) facilitating the assessment of different scenarios are devised. The following dimensionless indicator based on oil recovery factor (RF) and cumulative steam-to-oil ratio (CSOR) is implemented:

$$R = RF/CSOR \quad (3-4)$$

Where $RF = COP/OOIP = \text{cumulative oil production/original oil in place}$ and $CSOR = \text{cumulative steam-to-oil ratio}$. It is observed that neither RF nor $CSOR$ alone is sufficient as a comprehensive performance indicator; for example, there are scenarios in which low $CSOR$ is a result of low injectivity (and hence low production).

The measure that is based on the concept of discounted barrel of oil is also explored. It takes into account the economic impact of steam consumption and variation in fluid properties. In the simplest terms, it represents the net energy that can obtain from the process. Assumptions and calculation procedures are detailed in the **Appendix B**.

Another important variable in describing the efficiency of steam injection is t_{iSOR} , which is defined as the duration over which the monthly average steam-to-oil ratio ($iSOR$) exceeds 5 (a commonly-accepted upper limit for typical SAGD wells). For a given value of COP , low values of t_{iSOR} and $CSOR$ would correspond to higher steam injection efficiency. A dimensionless form defined as $t_{DiSOR} = t_{iSOR} / t_s$ is considered as an output attribute in the ANN modeling.

3.4 Artificial Neural Network for Data-Driven Model

In this thesis, ANN is used to analyze the simulation results by correlating the inputs and outputs. Therefore, the formulation and architecture of ANN is briefly introduced in this section.

A schematic of various elements of an ANN consisting of only one hidden layer has been illustrated in Fig. 2-1. In a back-propagation neural network (BPNN), signal is

passed from an input layer of neurons through a series of hidden layer to an output layer of neurons, while error is back propagated from the output layers to train the unknown network parameters including weights and biases (Bishop 1995). The input signals are multiplied by their corresponding weights to obtain the value of Y:

$$Y_j = w_0 + \sum_{i=1}^n w_{ij}x_i , \quad (3-5)$$

Where Y_j is weighted sum of input signals at node j ; w_0 is threshold (bias) value; w_{ij} is the weight associated with the connection between node j and the input node i ; x_i = value of input node i ; and n = number of input nodes. An activation function such as the one shown in **Eq. 3-6** is applied to the weighted sum:

$$f(Y) = \frac{1}{1 + e^{-Y}} \quad (3-6)$$

The output signal from node j is calculated from Eq. 3-6, and it is considered as the input signal to the next layer. Eqns. 3-5 and 3-6 are applied repeatedly until the final output layer is reached and the value for the target variable is computed. Because of large disparity in scales of different data sources, normalization or standardization procedures are performed on all input and output attributes (Francis 2001). The training data set is also used to design the optimal network configuration. Readers may refer to additional reference materials for ANN techniques (Zupan 1994; Shahab 1995; Shahab 2000; Al-Fattah and Startzman 2001; Weiss et al. 2002).

3.5 Principle Component Analysis

Principal component analysis (PCA) is performed to reduce the dimensionality of the original dataset (\mathbf{X}) through a linear projection onto a lower-dimensional subspace. A mean-adjusted dataset (\mathbf{Z}) is attained by subtracting the mean of each variable in \mathbf{X} . Next, the covariance between two variables are calculated to eliminate bias due to large disparity in mean values.

$$COV(X_j, X_k) = \frac{\sum_{i=1}^M Z_{ij}Z_{ik}}{M-1} \quad (3-7)$$

Where X_j and X_k represent two particular variables in \mathbf{X} ; M denotes the total number of samples in \mathbf{X} . The calculation in **Eq. (3-7)** is repeated for all pairs of variables to compute the covariance matrix, which is subjected to eigenvalue decomposition. Individual eigenvalue signifies the contribution of the variance from the corresponding eigenvector to the total variance of the original data. The eigenvectors with highest eigenvalues, or the principal components (PC), can be obtained by sorting the eigenvalues in decreasing order. Principal scores (PS), which are regarded as new inputs attributes in subsequent ANN modeling, are computed using **Eq. (3-8)**.

$$PS = PC \times Z^T \quad (3-8)$$

The detailed procedure of PCA is shown as follows:

1. Suppose n data and p variables are available and they form a matrix $[X]_{n \times p}$;
2. Subtract the mean from each of the p dimensions, get the new matrix $[Z]_{n \times p}$;
3. Calculate the covariance of the new matrix, $C = cov(Z)$;

4. Calculate the eigenvalue T and the eigenvector V , $[T, V] = \text{eig}(C)$;
5. Sort the eigenvalues from the maximum to minimum;
6. Select the first d eigenvalues and the corresponding eigenvectors which is considered as the principal components, create the matrix $[L]_{p \times d}$;
7. Calculate the final matrix $B = Z \times L$;
8. The B is the matrix after dimension reduction.

3.6 Sensitivity Analysis of Grid Size

To assess the impacts of grid sizes on the simulation accuracy and numerical dispersion, a sensitivity study is performed with three models with different cell sizes ($\Delta x \times \Delta y$): $1\text{m} \times 1\text{m}$ (coarse), $0.5\text{m} \times 0.5\text{m}$ (medium), $0.25\text{m} \times 0.25\text{m}$ (fine), respectively. Zones with high water saturation are commonly encountered underlying or overlying a heavy oil bearing formation such as those in Alberta (Kendall 1977; Towson 1977; Law, et al. 2003). Although a gas cap near the top of the reservoir is rarely observed, high gas saturation can be a result of natural depletion (Farouq Ali, 1983). Pooladi-Darvish and Mattar (2002) reported that top water leads to more-severe heat loss than a top-gas cap because of higher heat capacity of water. They also suggested that top water could drain into and collapse the steam chamber. Therefore, in this study, effects of a gas cap were not considered. All three models consist of a 3-m top water zone and a 4-m bottom water layer. There are seven shale barriers randomly distributed in the reservoir, but their sizes and positions are kept constant among the three cases. Simulation results show that only

minor difference (less than 0.002%) in cumulative production after 20 years is observed. However, significant differences in computational costs are noted: by use of a 3.4 GHz, 16GB of RAM, Intel Core i7-2600 CPU, the execution time for the model with $0.25\text{m} \times 0.25\text{m}$ cell size is 9.6 times and 576 times longer than that of the $0.5\text{m} \times 0.5\text{m}$ model and $1\text{m} \times 1\text{m}$ model, respectively. Balancing both accuracy and computational efficiency, a cell size of $1\text{m} \times 1\text{m}$ is selected in this study.

Table 3-1 Parameters in Eqn. (3-1)

Parameters	Value	Unit
a_o	11	-
a_w	21	-
c_o	-7.5×10^{-7}	-
c_w	1.0×10^{-6}	-

Table 3-2 Reservoir and Fluid Properties

Parameters	Value	Unit
Reservoir Depth	200	m
Reservoir Pressure	1500	kPa
Reservoir Width	900	m
Horizontal Permeability	5	D
Reservoir Temperature	18	°C
Oil Viscosity (18 °C)	600,000	cp
Rock Compressibility	9.6×10^{-6}	kPa^{-1}
Formation Heat Capacity	2350	$\text{kJ/m}^3 \cdot \text{K}$
Rock Thermal Conductivity	6.6×10^5	$\text{J/m} \cdot \text{d} \cdot ^\circ\text{C}$
Oil thermal Conductivity	1.15×10^4	$\text{J/m} \cdot \text{d} \cdot ^\circ\text{C}$
Water Thermal Conductivity	5.35×10^4	$\text{J/m} \cdot \text{d} \cdot ^\circ\text{C}$
Gas Thermal Conductivity	1.4×10^2	$\text{J/m} \cdot \text{d} \cdot ^\circ\text{C}$

Table 3-3 Parameters in Archie Equation

Parameter	Clean sand	LQS	Shale	Unit
a	1	1	1	-
m	2	2	2	-
n	2	2.5	3	-
R_t	500	300	100	$\Omega \cdot \text{m}$
R_w	0.2	0.2	0.2	$\Omega \cdot \text{m}$

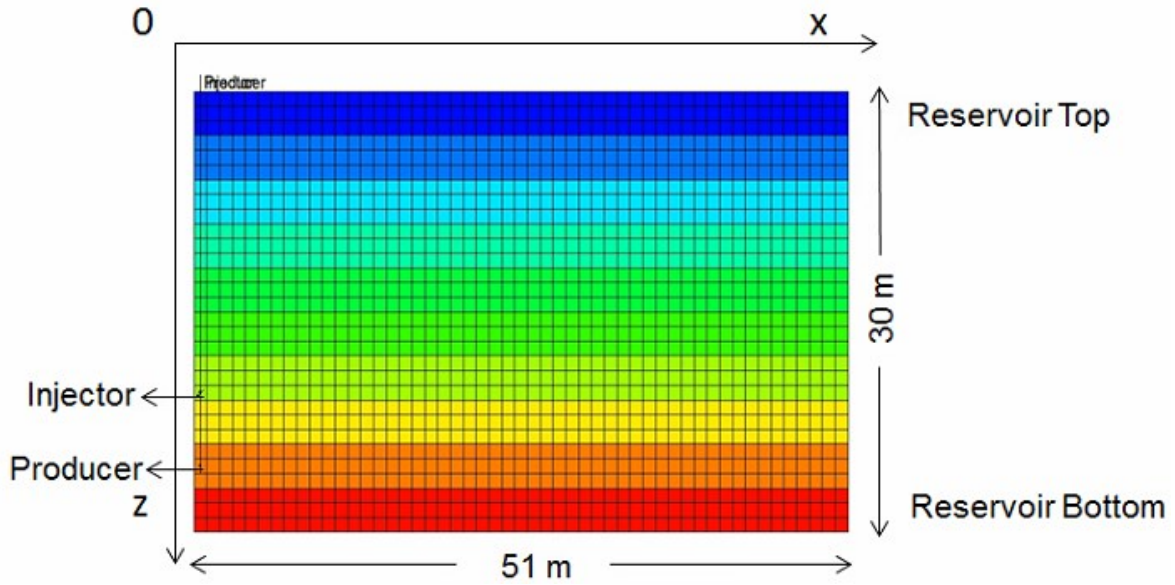


Figure 3-1(a) Configuration and setup for 2D (X-Z plane) SAGD simulation.

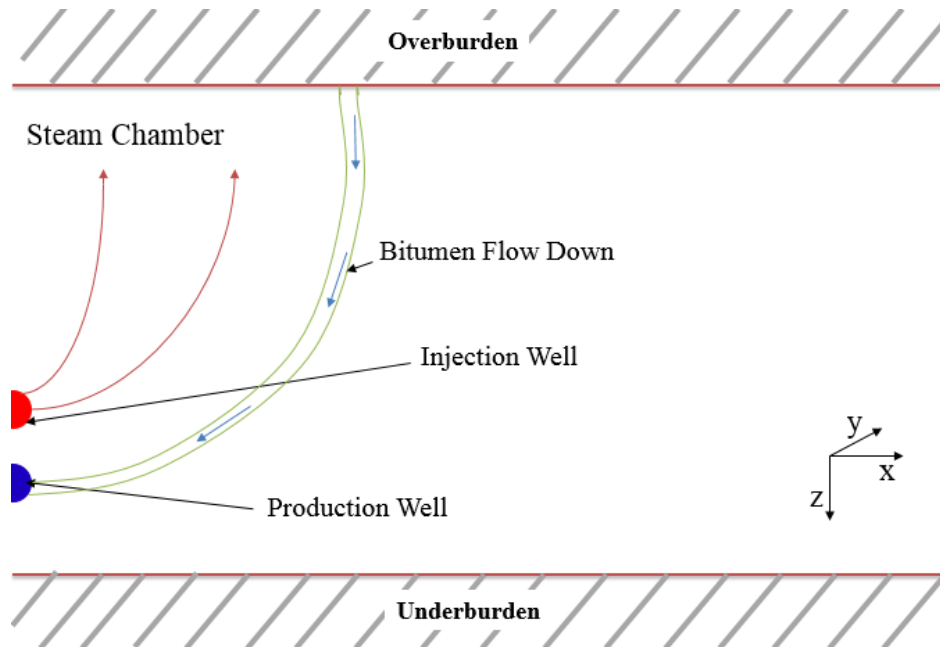


Figure 3-1(b) Schematic of steam chamber expansion in a SAGD displacement.

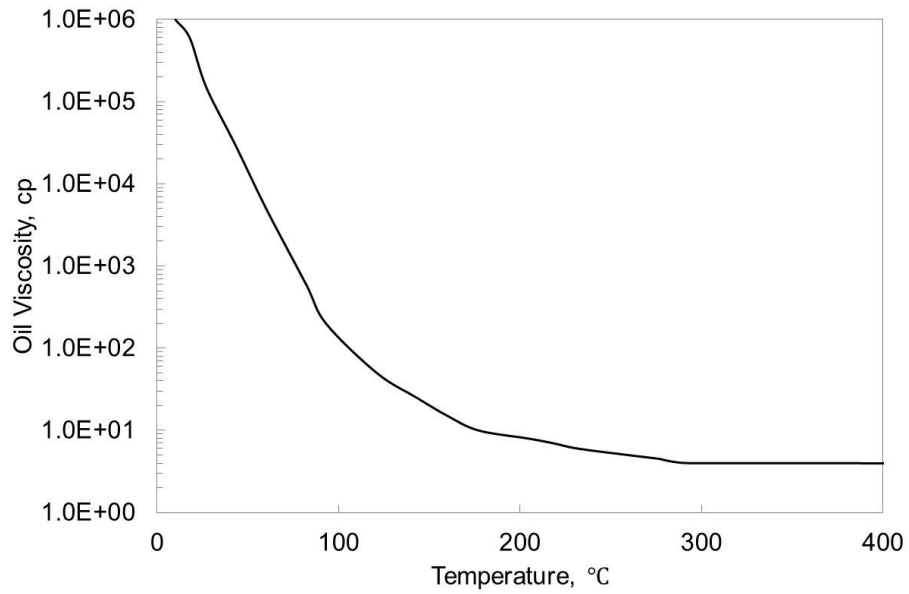


Figure 3-2 Oil viscosity profile as a function of temperature.

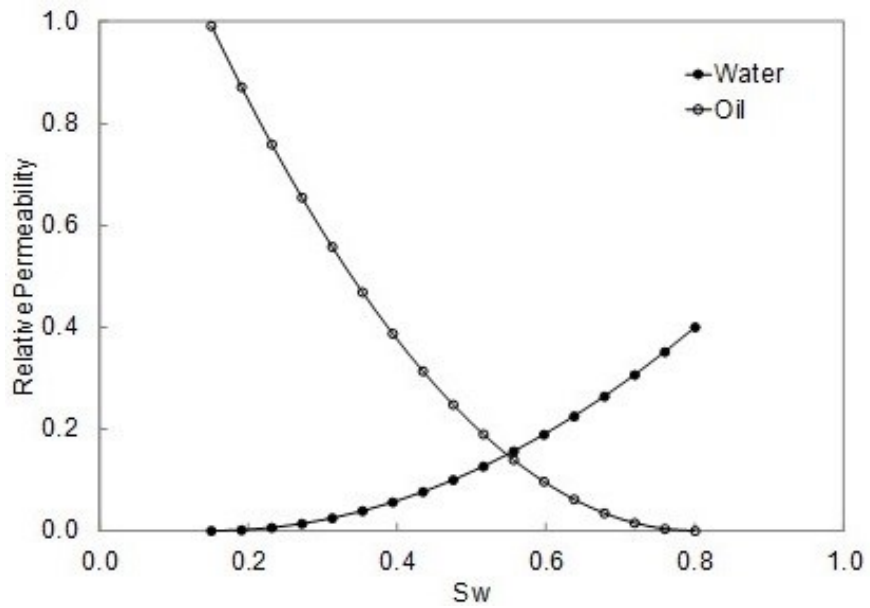


Figure 3-3(a) Relative permeability functions in clean sand and LQS for water-oil system.

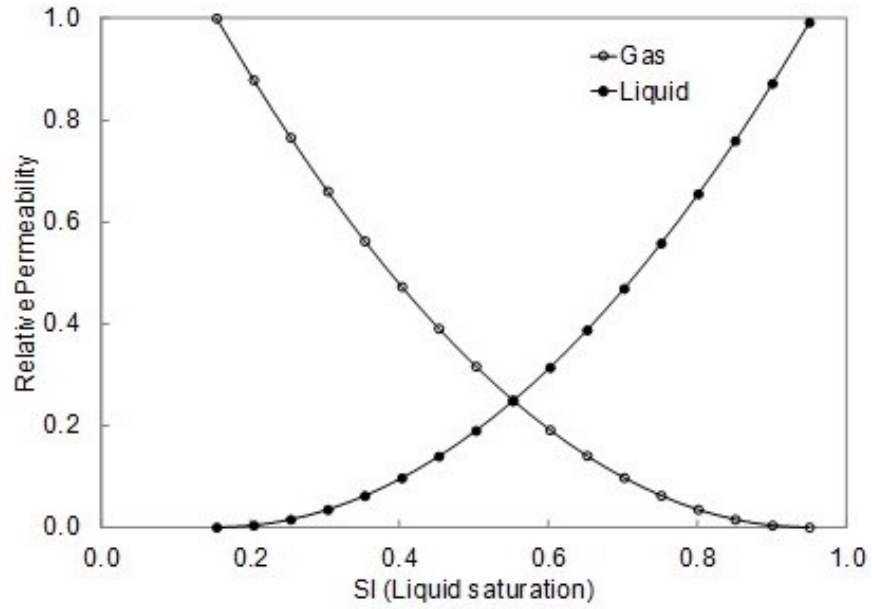


Figure 3-3(b) Relative permeability functions in clean sand and LQS for liquid-gas system.

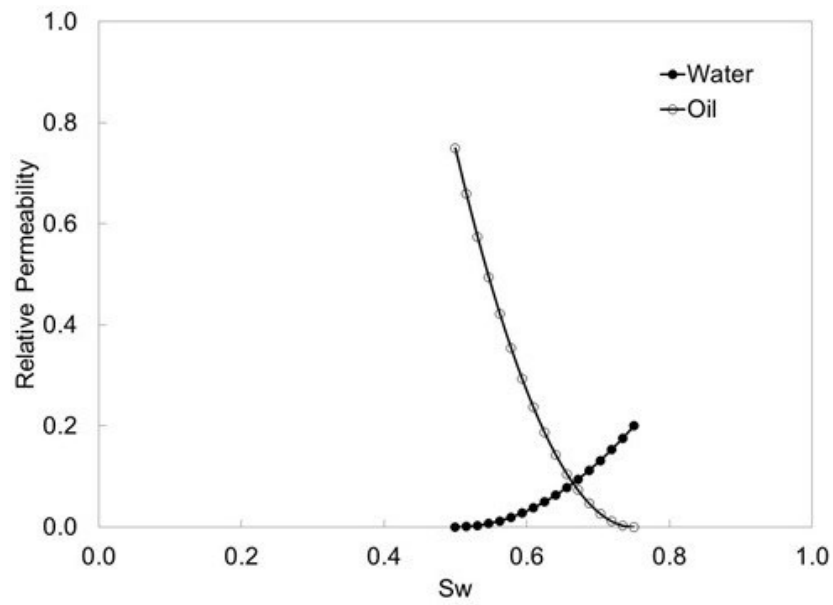


Figure 3-4(a) Relative permeability functions in shale barrier for water-oil system.

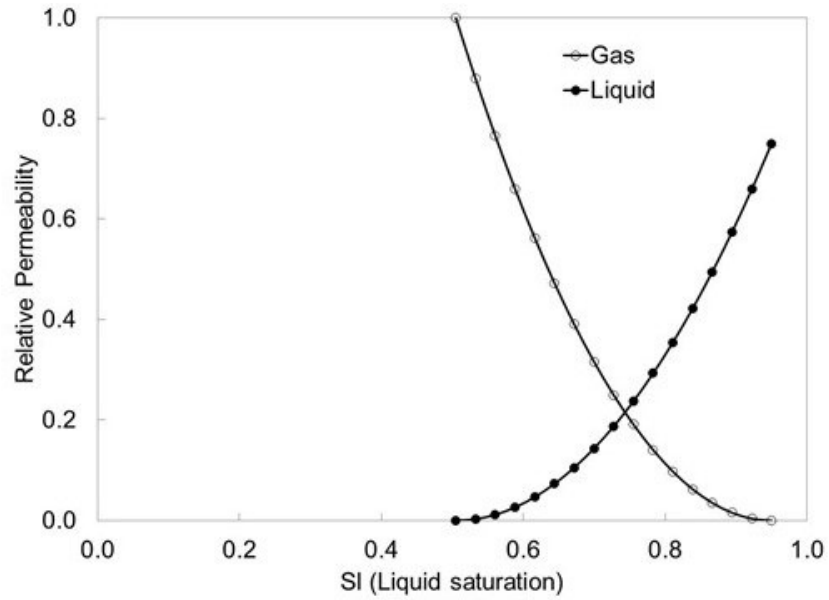


Figure 3-4(b) Relative permeability functions in shale barrier for liquid-gas system.

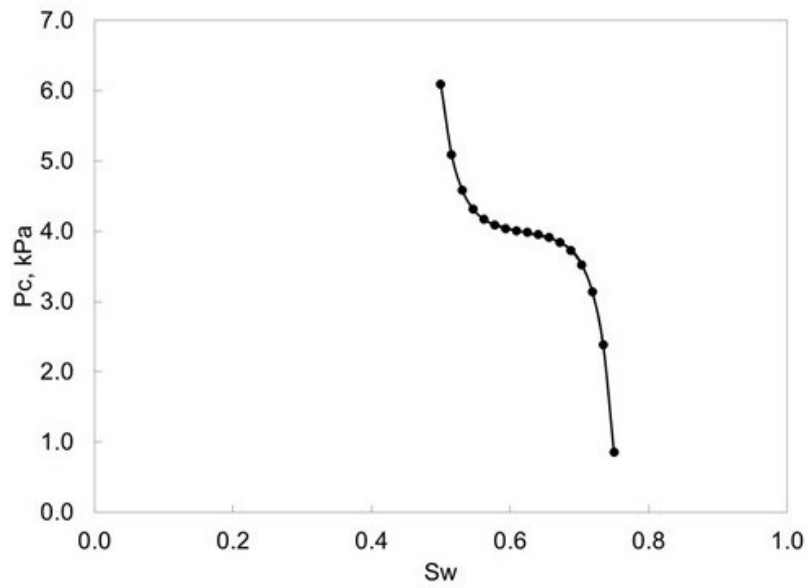


Figure 3-5 Capillary pressure functions for water-oil system in shale barrier.

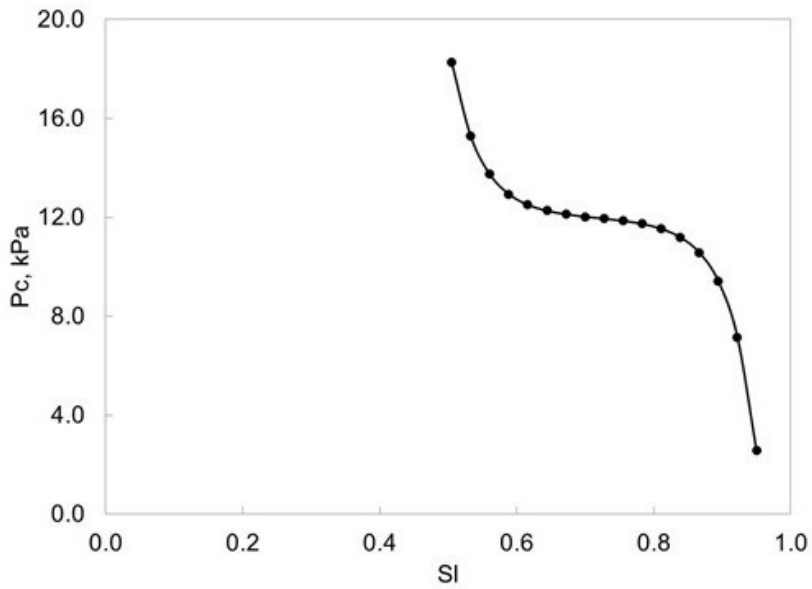


Figure 3-6 Capillary pressure functions for liquid-gas system in shale barrier.

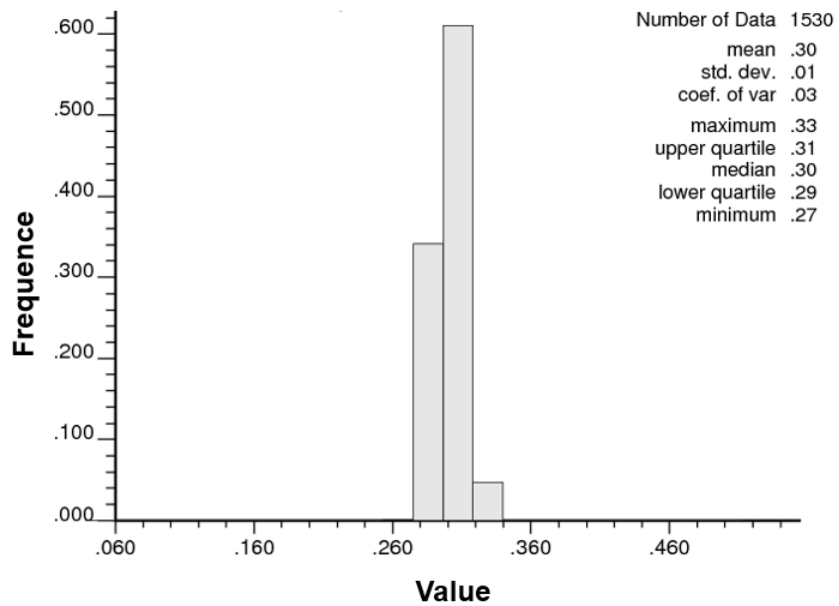


Figure 3-7(a) Histogram of porosity for clean sand by use of SGSIM.

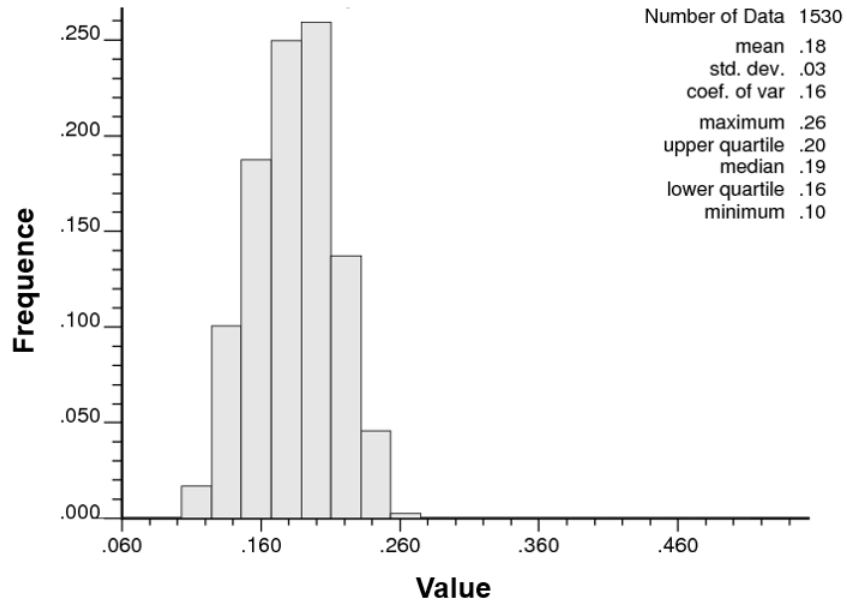


Figure 3-7(b) Histogram of porosity for LQS by use of SGSIM.

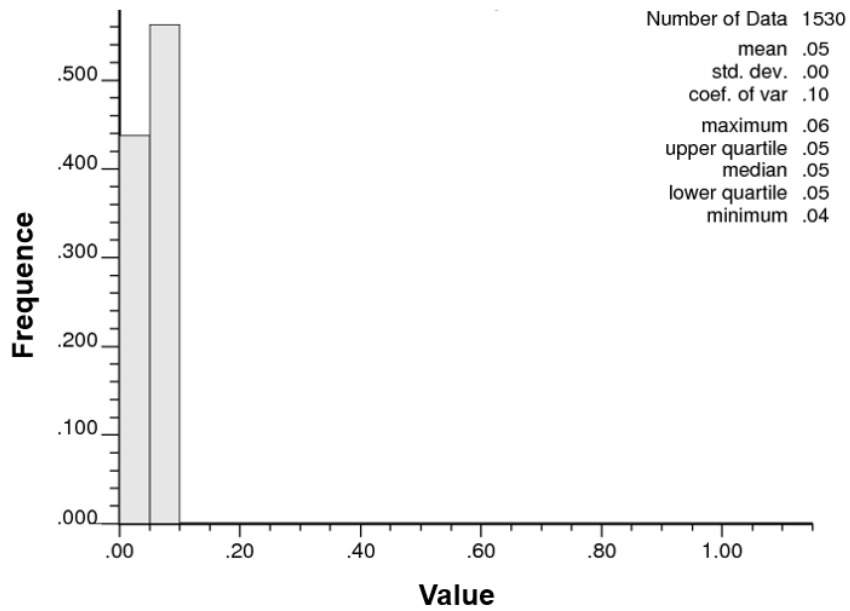


Figure 3-7(c) Histogram of porosity for shale barrier by use of SGSIM.

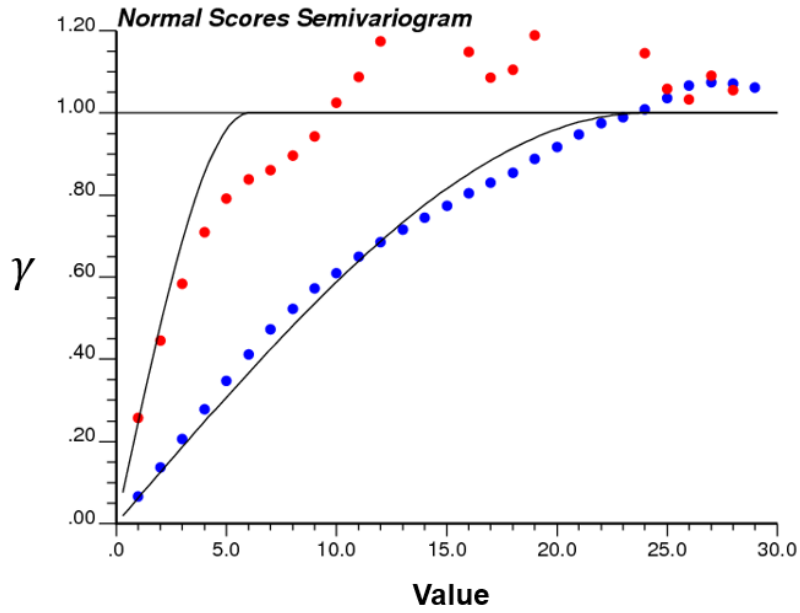


Figure 3-7(d) Variogram of porosity distribution for clean sand, LQS, and shale barrier by use of SGSIM.

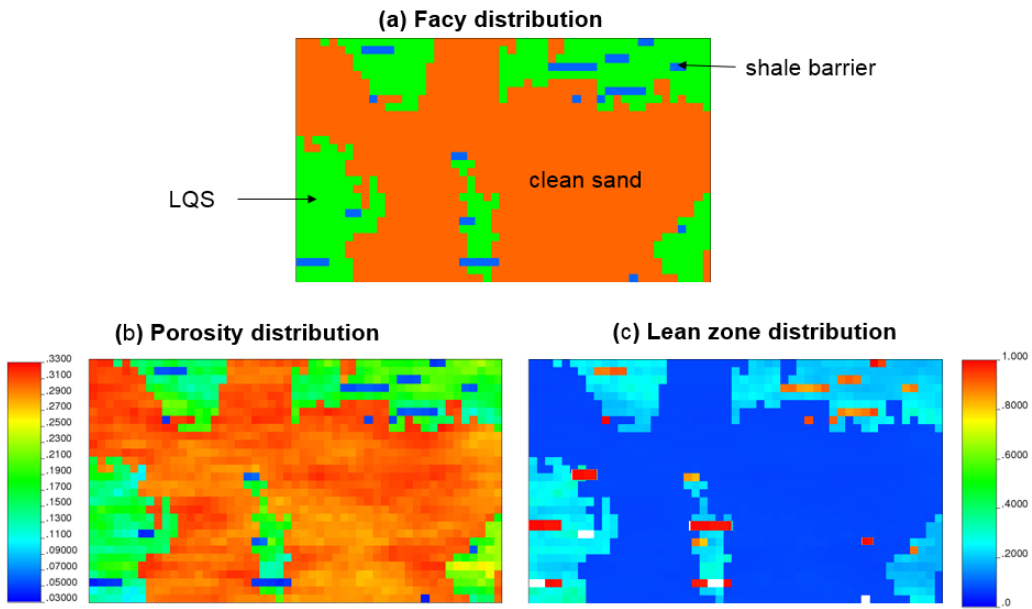


Figure 3-8 Distribution for clean sand, LQS and shale barriers, and corresponding porosity, water saturation distribution.

Chapter 4: Assessing Impacts of Reservoir Heterogeneities on SAGD Performance

In this chapter, detailed sensitivity analysis is performed to explore the effects of reservoir heterogeneities of shale and lean zone on SAGD performance, which helps find the important parameters associated with SAGD performance. Effects of shale and lean zone in reservoir on SAGD are investigated in terms of location, continuity, size, proportion and saturation.

4.1 Effects of Lean Zones on SAGD Performance

In this sub-section, the effects of lean zones, which are defined as layers consisting of reduced oil saturation that are overlying (top water) or underlying (bottom water) the pay zone, are investigated. A base case is set up without any lean zone.

4.1.1 Top Water

A sensitivity analysis is carried out by increasing the water zone thickness. Results of RF, CSOR, DB and R are shown in **Table 4-1** as a function of dimensionless water zone thickness defined as $h_{Dwt} = H_{wt}/H$, where H_{wt} is the thickness of top water zone and H is the reservoir thickness. **Fig. 4-1** compares the oil saturation distribution after 2 years for four selected cases with H_{wt} less than 10 m ($h_{Dwt} = 0.3333$). At the end of the preheating period, the steam chamber grows vertically and mobilizes the oil uniformly with essentially zero bypassed oil. When the steam chamber reaches to the top of the pay zone,

the injected steam is used to vaporize the top water layer, which serves as a thief zone. Despite the heat loss through the top water, the additional steam helps to accelerate the steam chamber expansion. As shown in Fig.4-1, the steam chamber expands more quickly as the top water thickness increases. This is corroborated by the acceleration in oil production with top water thickness. A key observation is that thicker top water zone absorbs more heat and requires more steam injection, resulting in a higher CSOR as shown in Table 4-1. This observation, similar to that in Pooladi-Darvish and Mattar (2002) and Law et al. (2003), suggests that heat transfer to the oil is most efficient when steam remains in the pay zone instead of the surrounding formation. Law et al. (2003) compared oil rate and CSOR for three scenarios including (1) absence of top water, (2) confined top water and (3) unconfined top water. It was observed that oil rate increased in the presence of confined top water. However, no sensitivity analysis regarding the thickness of the confined top water was performed in that study; hence no complete systematic conclusion regarding effect of top water on SAGD performance could be derived. Nasr et al. (2000) also concluded from experimental studies that the thicker top water zone would lead to higher CSOR. The ranking results in terms of R and DB shown in Table 4-1 demonstrate further a reduction in process efficiency as h_{Dwt} increases. Collapsing of the steam chamber is not observed from this simulation study, which is in agreement with other previous studies (Good et al. 1997).

To model an unconfined aquifer overlaying the reservoir with constant pressure boundary condition, a series of water injectors with constant bottom-hole pressure

constrained at the initial reservoir pressure are positioned near the top. As the oil drains, water encroachment into the reservoir, which is detrimental to steam chamber expansion and the ensuing oil production, becomes prevalent. However, this negative impact on COP is not observed for the cases with confined top water. As a result, the overall SAGD performance with unconfined top water is much worse than the base case in terms of R and DB values. One should note that Law et al. (2003) also reported the highest CSOR for the unconfined case, which is consistent with this study. Next, a series of simulations are performed with varying levels of oil saturation in top water zone for a fixed 5m thickness. Simulation and ranking results are summarized in Table 4-1. The presence of oil in top water zone is beneficial for the SAGD performance in terms of values of R and DB. As the oil saturation in top water increases from 0 to 0.95, the efficiency of SAGD process increases by 32% in terms of R.

4.1.2 Bottom Water

A sensitivity analysis is carried out by increasing the water zone thickness. Results of RF, CSOR, R and DB are shown in **Table 4-2** as a function of dimensionless water zone thickness defined as $h_{Dwb} = H_{wb}/H$, where H_{wb} is the thickness of bottom water zone and H is the reservoir thickness. **Fig. 4-2** compares the oil saturation distribution after 5 years for 4 selected cases. When the steam chamber rises, the water in the bottom layer begins to flow toward the production well because of its low viscosity. Because steam chamber expansion is primarily localized in regions above the producer, the presence of bottom

water has minor effect on the shape or advancement of the steam chamber and the ensuing oil mobilization within the chamber; however, the mobilized oil would drain into the bottom water zone because of gravitational force and thus increase the oil saturation at depths below the producer. The low oil saturation region near the lower left corner is caused by coning. Because water production is driven by the pressure difference, the heated oil is drained along the steam chamber to the producer, as well as to the bottom zone to replace the void space left by the produced water. On the other hand, the low oil saturation region in the lower right hand corner is present only at early time (before the steam chamber reaching the right boundary). After all oil is mobilized by the steam (e.g., after 10 years in our cases), this low oil saturation region would disappear. To investigate the sensitivity of well control, simulations are performed with various pressure differences between injector and producer: 200, 400 (base case) and 800 kPa. Less than 10% difference in results (R values and oil saturation distribution) is observed among these cases. Because SAGD operation optimization is not a primary focus of this work, all simulations are conducted with the same well control as in the base case. In addition, the water production from the lean zone has increased the water cut at the producer, resulting in a lower oil rate. These mechanisms would explain the lower RF observed for the case with thicker bottom water as shown in Table 4-2. The ranking results also suggest that increase in bottom water thickness reduces the performance efficiency significantly, and the effect appears to be more severe than for the top water scenario. A lean zone below the producer does not introduce additional benefits of enhancing steam

chamber advancement and subsequent oil recovery; instead, it serves as an energy sink, which increases the CSOR eventually. To model a scenario in which the reservoir is underlaid by an unconfined aquifer with constant pressure boundary condition, a series of water injectors with constant bottom-hole pressure constrained at the initial reservoir pressure are positioned near the bottom. Much more water is flowing into the producer, leading to a higher water cut and lower oil recovery.

Next, a series of simulations is performed with varying levels of oil saturation in bottom water zone for a fixed 5m thickness. Simulation and ranking results are also summarized in Table 4-2. Similar to the cases of top water, higher oil saturation in the bottom water contributes to the higher R and DB. As the oil saturation in bottom water increases from 0 to 0.95, the efficiency of SAGD process increases by 34% in terms of R.

4.2 Effects of Shale Distribution on SAGD Performance

In this subsection, a comprehensive analysis about the continuity, location, size (length scale and thickness), and proportion of the shale barriers is presented. First, a base case is set up with clean sand only, in which capillary pressure effects are neglected. Next, the effects of LQS with a single continuous shale barrier are studied (**Fig. 4-3 a-b**). Finally, sensitivity of the location and distribution of discontinuous shale barriers is explored in (**Fig. 4-3 c-d**).

To assess the impacts of capillary pressure, results for a single shale barrier (**Fig. 4-3a**) are repeated with and without capillary pressure effects. **Fig. 4-4** compares the oil

rate and monthly average steam-to-oil ratio (iSOR) with/without capillary pressure effects. An increment of 3% for COP is observed caused by a slightly higher oil rate at early production stage, if capillarity effect is ignored. The effect on iSOR is more observable during the later production period; an increment of 4.2% for CSOR is detected for the case without capillarity effect. Considering that most models used in this work consist of shale proportions much higher than those in Fig. 4-3a, one should not ignore the impacts of capillary pressure.

4.2.1 Continuous Shale Barrier

Fig. 4-3b illustrates the configuration of a single continuous shale barrier with LQS. Positions of the shale barriers in relation to the well pair are varied systematically according to three categories: (a) AIR: above the injector region, (b) BIP: between injector and producer, (c) UPR: underneath producer region. A series of simulations cases is performed by varying the position of the shale barriers: $z = 3, 10, 17$ (AIR); $z = 22, 23, 24$ (BIP); and $z = 27, 28, 29$ (UPR). Simulation and ranking results are summarized in **Table 4-3** (without LQS) and **Table 4-4** (with LQS). The length (L_{sh}) and thickness (H_{sh}) of the shale barrier are expressed dimensionlessly as: $l_{Dsh} = L_{sh}/L$ and $h_{Dsh} = H_{sh}/H$, where L refers to the length of the reservoir.

It is interesting to note that the incorporation of LQS does not have a significant adverse effect on the ultimate oil production and CSOR. Values of RF, CSOR, R and DB shown in Tables 4-3 and 4-4 suggest that only minor reduction in recovery efficiency is

detected when LQS is modeled. This observation is also corroborated by the comparison of RF and CSOR profiles in **Fig. 4-5** for a single shale barrier at $z = 10$ in cases with and without LQS. A possible explanation is that properties (porosity, permeability, and multiphase flow functions) assigned to the LQS in this study are approximately the same as those in the clean sand; therefore, the LQS would not strongly impede steam chamber expansion and the fluid drainage toward the production well. In addition, the areal extent of the LQS is rather limited. In fact, under certain circumstances, reduced velocity in the LQS would lead to a more uniform chamber front and slightly higher RF. Although the focus of this current study is the heterogeneity in shale barrier distribution, further sensitivity analysis is required to fully capture impacts of LQS characteristics in SAGD performance.

Next, **Fig. 4-6** compares the oil saturation distribution with different locations of the single continuous shale barrier with LQS after 5 years. When the nearly impermeable shale barrier is located at $z = 10$ in the region above the injector (AIR), the vertical growth of the steam chamber is strongly impeded, compelling the steam to spread sideways underneath the shale barrier, which is acting like a cap rock. As a result, the oil above the shale barrier is bypassed. On the other hand, if the shale barrier is at $z = 28$ in the region beneath the producer (UPR), the shale barrier essentially has a very minor impact on the recovery process. Values of its performance indicators of R and DB are the same as those in the base case, though RF and CSOR values have both increased slightly.

When the shale barrier is between the injector and producer (BIP: e.g., $z = 23$), steam

injection and chamber advancement are significantly hampered, hindering oil production toward the producer. Although the shale barrier does not interfere with the vertical growth of the steam chamber, permitting heat transfer and the oil to be mobilized above the injector, it is, however, obstructing the heated oil from draining toward the producer.

The RF and CSOR profiles for the three cases are shown in **Fig. 4-7**. Because of the obstruction of the shale barrier in the AIR, the RF in the case of $z = 10$ is lower than the base case. Because the shape of the steam chamber is distorted around the shale barrier, increased bypassed oil above the shale barrier contributes to a higher CSOR. A combination of reduced RF and increased CSOR would ultimately result in a lower R value in Table 4-4. As the shale barrier is placed closer to the injector, the amount of bypassed oil increases, reducing the efficiency (and ranking) of the ensuing SAGD process. When the shale barrier is at $z = 28$ below the producer, the corresponding RF and CSOR profiles are very similar to those in the base case. Finally, when the shale barrier is at $z = 23$ in between the well pair, both the RF and ranking drop dramatically despite the fact that the CSOR is much lower than the base case. Steam injectivity is dramatically reduced because of this extremely low production.

On the basis of the aforementioned observations, one can deduce a number of general conclusions regarding the impacts of shale barriers on SAGD performance. First, shale barriers above the injector could impede the advancement of steam chamber. Second, all shale barriers, regardless of their positions or distributions, could obstruct oil drainage towards the producer. Finally, evaluation of the SAGD performance should be

facilitated with some ranking indicator or scheme that takes into account both RF and CSOR. It is demonstrated in a number of cases in which either CSOR or RF is enhanced as compared to the base case, whereas the overall performance efficiency is notably inferior.

4.2.2 Discontinuous Shale Barrier

Fig. 4-3c illustrates the configuration of a single discontinuous shale barrier with LQS. A series of simulation cases is performed by varying the position of the shale barrier: $z = 3, 10, 17$ (AIR); $z = 22, 23, 24$ (BIP); and $z = 27, 28, 29$ (UPR) – same as in the preceding subsection. Each segment of the shale barrier has a uniform length of 3 m ($l_{Dsh} = 0.5882$). Results of the simulation and ranking are also shown in Table 4-4.

Although the shale barriers could still hinder the expansion of steam chamber and increase the amount of bypassed oil inside the steam chamber, their impacts are significantly diminished as the continuity reduces. Shale barriers of shorter length scale allow the steam chamber to expand around them. Results in Table 4-4 also reveal that the performance (ranking) of all these cases is comparable to that in the base case. Once again, when the shale barrier is below the producer, their impacts on the subsequent performance are the least observable. It is interesting to note that sensitivity of shale position within a particular region (e.g. AIR) decreases as shale barrier continuity is reduced.

Results from the preceding subsection have provided a systematic understanding of

the various characteristics of shale distribution (location and continuity) on SAGD performance. Next, the effects of their length scale and thickness are investigated. In particular, a set of randomly distributed discontinuous shale barriers with LQS (a more realistic scenario) is used. The position of the shale barriers is generated stochastically. Fig. 4-3d shows a particular realization with 10 discontinuous shale barriers that are distributed randomly across the domain. Practically, depositional environment has a strong relationship with shale volume (Goetz et al. 1977), which can be reflected from the petrophysical log data; however, this relationship is not considered here. Instead, a series of sensitivity analyses is carried out by arbitrarily varying the length scale and thickness of the shale barriers.

A series of simulation cases is conducted with different shale barrier length scale, l_{Dsh} , while keeping the thickness constant at 1 m ($h_{Dsh} = 0.0333$), and the results are presented in **Table 4-5**. The oil saturation distributions after 5-year simulation are compared in **Fig. 4-8**. Additional oil is bypassed because the steam chamber interface is distorted by the shale barriers. As the length scale of shale barrier increases, distortion of the chamber interface and the fraction of bypassed oil also increase. This is evidenced by the reduction in RF and rise in CSOR shown in Table 4-5.

Next, another set of simulation cases is conducted in which the thickness of the randomly discontinuous shale barriers, h_{Dsh} , is varied while keeping the length scale constant at 5 m ($l_{Dsh} = 0.098$). The simulation results are summarized in **Table 4-6**. Comparison of oil saturation distributions with those in Fig. 4-8 reveals similar

characteristics; as the volume of the shale barriers increase, more oil is bypassed. This is always accompanied by a reduction in RF and an increase in CSOR. However, it is not obvious whether the thickness or length scale would be a more dominant factor in controlling the amount of bypassed oil, because this might depend on the shale properties in a specific reservoir.

Results in Tables 4-4 through 4-6 are corroborated by many previous studies of analyzing reservoir-heterogeneity effects on SAGD (Pooladi-Darvish and Mattar, 2002; Chen et al. 2008; Dang et al. 2010). It was typically shown that the presence of randomly distributed, discontinuous, thin shale/clay lenses with limited extent might not significantly affect production because heat conduction takes place without direct contact with the bitumen. One should note that variability in shale thickness was not studied in these previous works.

Table 4-1 Simulation Results for Cases with Top Water

h_{Dwt}	Top Water	RF	CSOR	R	DB (J/m ³)
	Oil Saturation			(RF/CSOR)	
0.0000	0	0.8523	1.683	0.506	3.79E+10
0.0333	0	0.8549	1.756	0.487	3.77E+10
0.1000	0	0.8552	1.858	0.460	3.75E+10
0.1667	0	0.8579	1.944	0.441	3.72E+10
0.2667	0	0.8598	2.062	0.417	3.69E+10
0.3333	0	0.8607	2.139	0.402	3.67E+10
unconfined	0	0.4363	28.192	0.015	5.01E+9
0.1667	0.05	0.8588	1.916	0.448	3.73E+10
0.1667	0.1	0.8594	1.888	0.455	3.74E+10
0.1667	0.15	0.8586	1.864	0.461	3.75E+10
0.1667	0.2	0.8594	1.834	0.469	3.75E+10
0.1667	0.5	0.8633	1.679	0.514	3.79E+10
0.1667	0.95	0.8605	1.479	0.582	3.85E+10

Table 4-2 Simulation Results for Cases with Bottom Water

h_{Dwb}	Bottom Water	RF	CSOR	R	DB (J/m ³)
	Oil Saturation			(RF/CSOR)	
0.0000	0	0.8523	1.683	0.506	3.79E+10
0.0333	0	0.8335	1.756	0.475	3.77E+10
0.1000	0	0.7942	1.904	0.417	3.73E+10
0.1667	0	0.7574	2.049	0.370	3.70E+10
0.2667	0	0.7092	2.285	0.310	3.63E+10
0.3333	0	0.6783	2.418	0.281	3.60E+10
unconfined	0	0.6776	2.8168	0.2405	3.53E+10
0.1667	0.05	0.7574	2.012	0.377	3.71E+10
0.1667	0.1	0.7609	1.997	0.381	3.71E+10
0.1667	0.15	0.7673	1.944	0.395	3.72E+10
0.1667	0.2	0.7667	1.933	0.397	3.73E+10
0.1667	0.5	0.7731	1.773	0.436	3.77E+10
0.1667	0.95	0.7813	1.575	0.496	3.82E+10

Table 4-3 Simulation Results for Single Continuous Shale Barrier without LQS

Location of Shale Barrier Layer(z)		l_{Dsh}	RF	CSOR	R (RF/CSOR)	DB (J/m ³)
Base Case		1	0.8523	1.683	0.506	3.79E+10
AIR	3	1	0.8104	1.798	0.451	3.76E+10
	10	1	0.6164	2.206	0.279	3.65E+10
	17	1	0.3887	3.105	0.125	3.41E+10
BIP	22	1	0.0021	0.281	0.007	4.17E+10
	23	1	0.0017	0.678	0.002	4.06E+10
	24	1	0.0014	1.818	0.001	3.76E+10
UPR	27	1	0.8599	1.705	0.504	3.79E+10
	28	1	0.8611	1.702	0.506	3.79E+10
	29	1	0.8637	1.711	0.505	3.79E+10

Table 4-4 Simulation Results for Single Continuous and Discontinuous Shale Barrier with LQS

Location of Shale Barrier Layer(z)		l_{Dsh}	RF	CSOR	R (RF/CSOR)	DB (J/m ³)
Base Case		0	0.8523	1.683	0.506	3.79E+10
AIR	3	1	0.8170	1.855	0.440	3.75E+10
	10	1	0.6251	2.280	0.274	3.63E+10
	17	1	0.3115	3.963	0.079	3.18E+10
BIP	22	1	0.0023	0.814	0.003	4.03E+10
	23	1	0.0016	1.418	0.001	3.86E+10
	24	1	0.0013	1.708	0.001	3.79E+10
UPR	27	1	0.8582	1.763	0.487	3.77E+10
	28	1	0.8807	1.742	0.506	3.78E+10
	29	1	0.8843	1.744	0.507	3.78E+10
AIR	3	0.0588	0.7996	1.779	0.449	3.77E+10
	10	0.0588	0.8038	1.797	0.447	3.76E+10
	17	0.0588	0.8039	1.812	0.444	3.76E+10
BIP	22	0.0588	0.8012	1.801	0.445	3.76E+10
	23	0.0588	0.8018	1.800	0.445	3.76E+10
	24	0.0588	0.8016	1.812	0.443	3.76E+10
UPR	27	0.0588	0.8422	1.697	0.496	3.79E+10
	28	0.0588	0.8360	1.720	0.486	3.78E+10
	29	0.0588	0.8353	1.731	0.483	3.78E+10

Table 4-5 Simulation Results for Randomly-Distributed Discontinuous Shale Barriers with LQS with Fixed Shale Barrier Thickness

l_{Dsh}	h_{Dsh}	RF	CSOR	R (RF/CSOR)	DB (J/m ³)
0	0	0.8523	1.683	0.506	3.79E+10
0.0196	0.0333	0.8277	1.733	0.478	3.78E+10
0.0588	0.0333	0.8077	1.785	0.452	3.77E+10
0.0980	0.0333	0.7919	1.816	0.436	3.76E+10

Table 4-6 Simulation Results for Randomly-Distributed Discontinuous Shale Barriers with LQS with Fixed Shale Barrier Length

l_{Dsh}	h_{Dsh}	RF	CSOR	R (RF/CSOR)	DB (J/m ³)
0	0	0.8523	1.683	0.506	3.79E+10
0.0980	0.0333	0.7948	1.820	0.437	3.76E+10
0.0980	0.1000	0.7391	1.930	0.383	3.73E+10
0.0980	0.1667	0.6848	2.088	0.328	3.69E+10

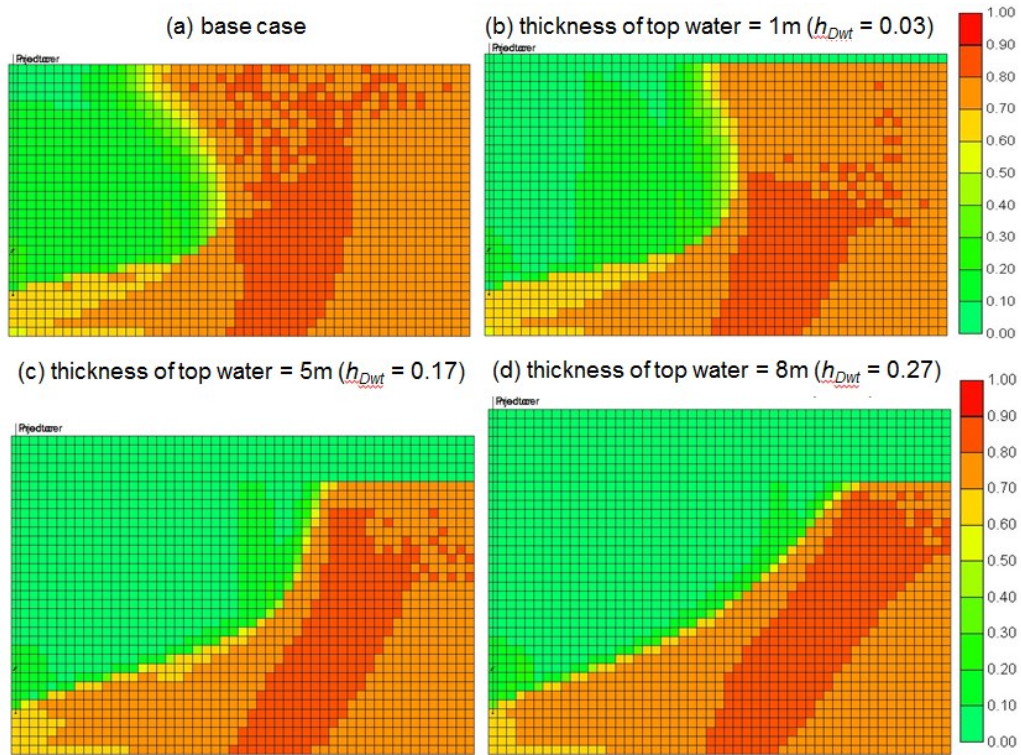


Figure 4-1 Oil saturation distribution after 2 years for varying top water thickness.

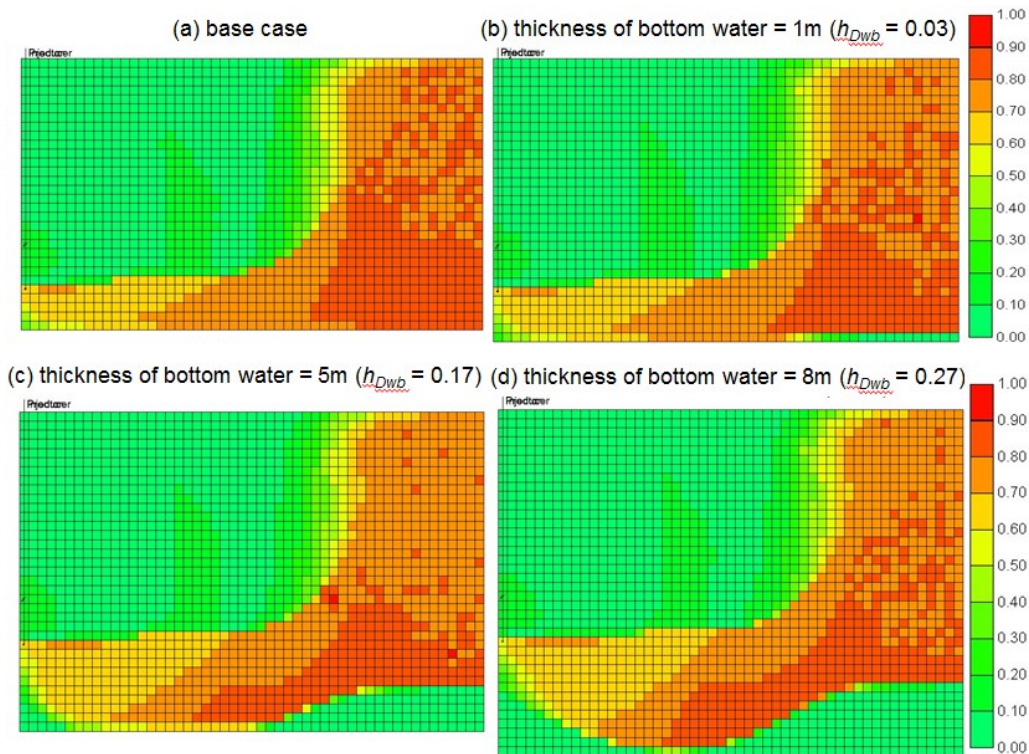


Figure 4-2 Oil saturation distribution after 5 years for varying bottom water thickness.

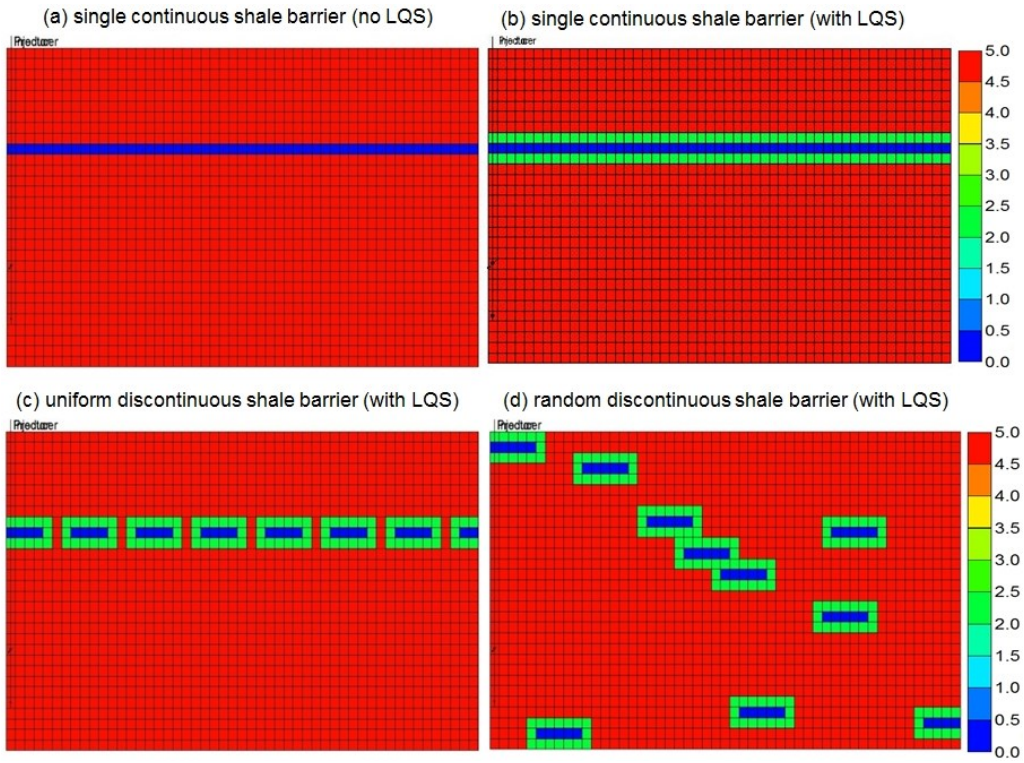


Figure 4-3 Permeability distribution (in darcies) for various shale distributions.

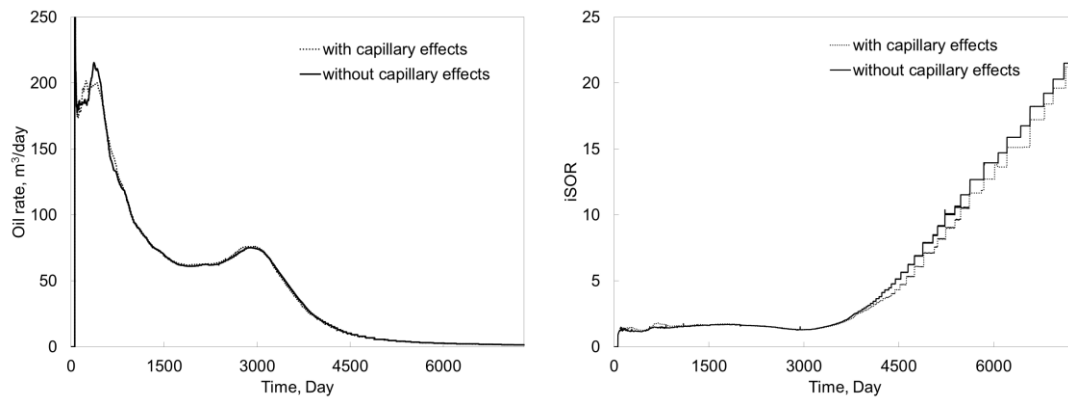


Figure 4-4 Impacts of capillarity on oil rate and iSOR over 20 years for a single continuous shale barrier located at $z = 10$.

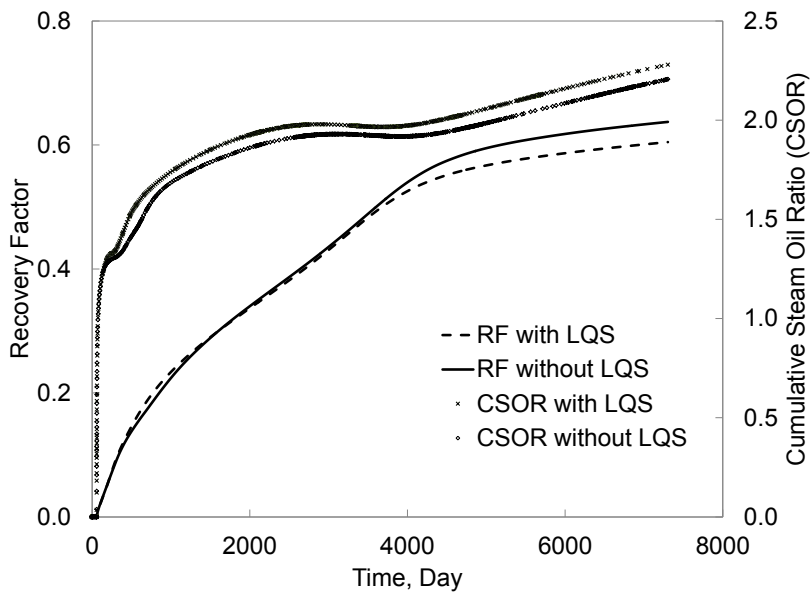


Figure 4-5 Comparison of RF and CSOR for 20 years for single continuous shale barrier at $z = 10$ with and without LQS.

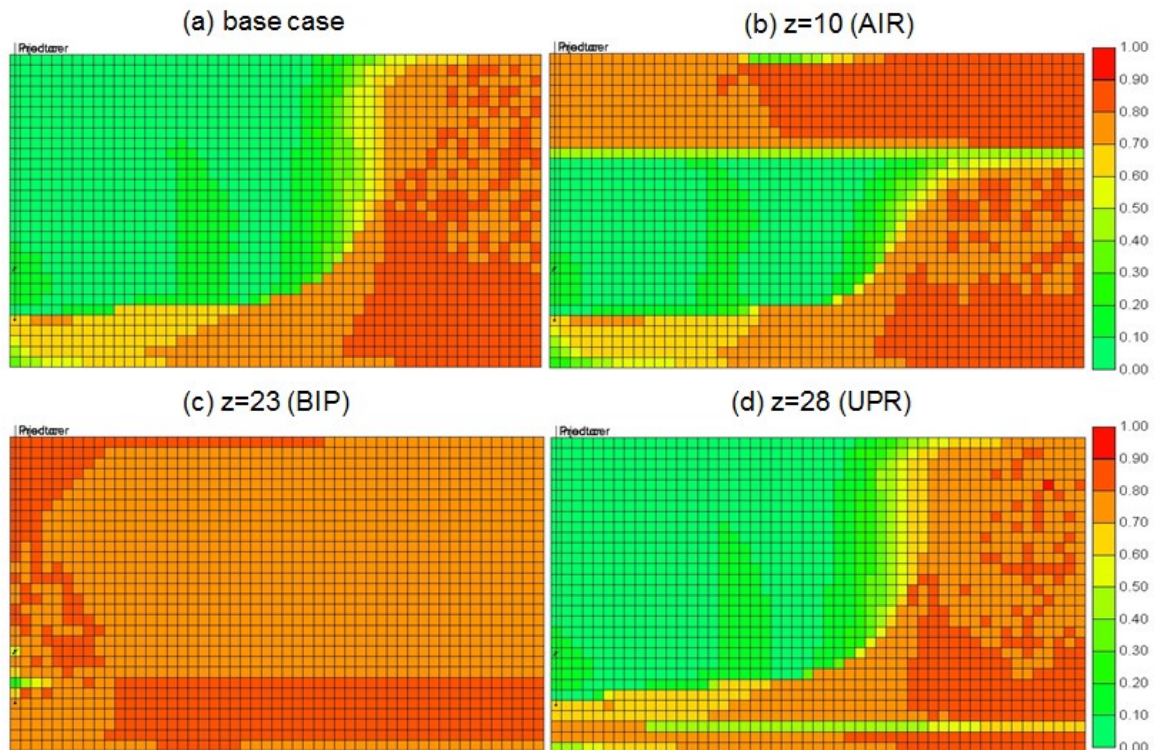


Figure 4-6 Oil saturation distribution after 5 years for different locations (z) of the single continuous shale barrier with LQS.

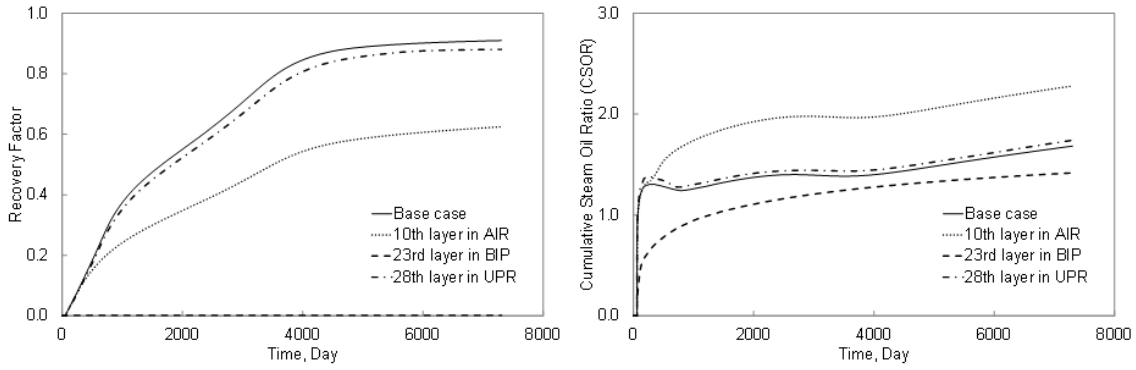


Figure 4-7 RF and CSOR for 20 years with different locations (z) of the single continuous shale barrier with LQS.

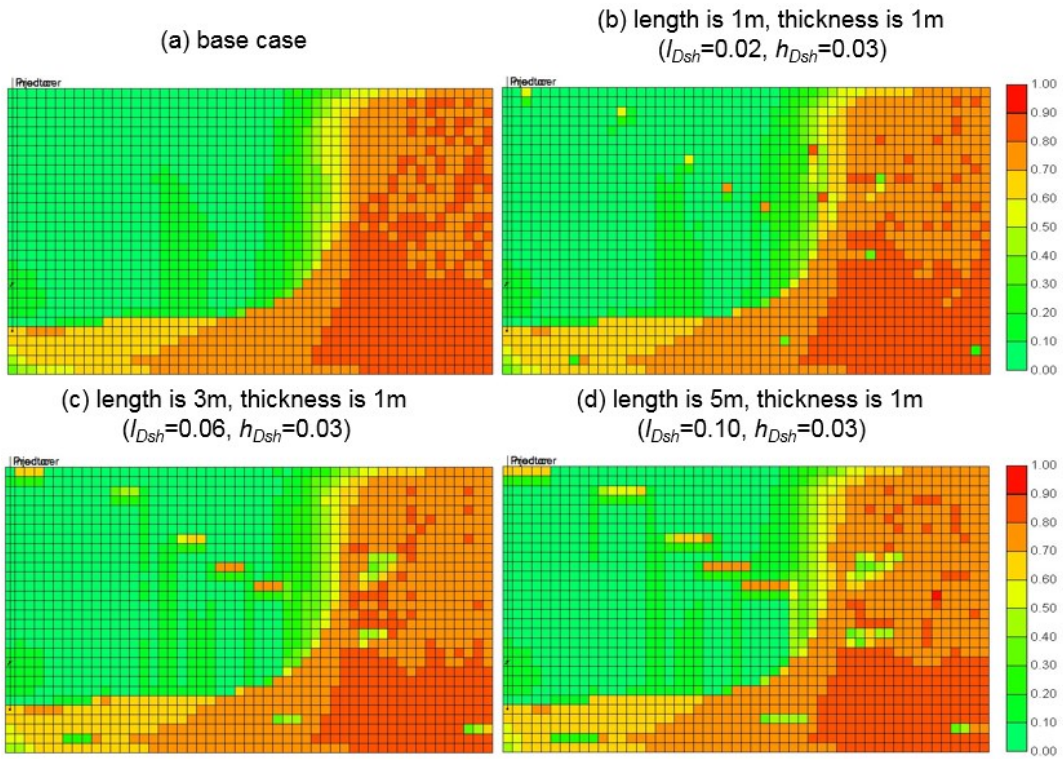


Figure 4-8 Oil saturation distribution after 5 years for different I_{Dsh} for randomly-distributed discontinuous shale barriers with LQS.

Chapter 5: Correlation of Reservoir Heterogeneities to SAGD

Performance Using Data-Driven Modeling Methods

In the chapter 4, a detailed sensitivity analysis is performed so that a comprehensive understanding about how shale barriers and lean zones affect the SAGD performance is obtained. In this chapter, the objective is to identify and propose a set of parameters suitable for characterizing the heterogeneities of shale layers and lean zones in SAGD reservoirs on the basis of the sensitivity analysis in chapter 4. ANN is used to develop a data-driven surrogate model to predict SAGD recovery performance from this set of heterogeneous reservoir variables.

This chapter starts with the correlation of reservoir heterogeneities to SAGD performance by use of the dataset from sensitivity analysis in chapter 4. Then, investigation of the correlation is extended to stochastic distribution of shale barriers and lean zones.

5.1 Correlation of Heterogeneity Attributes to SAGD Performance Indicators

Because of the complexity in the shale and lean-zone heterogeneities, it is hypothesized that simple parameters such as average porosity, permeability, or saturation would not suffice to capture the highly nonlinear relationship between these heterogeneous features and recovery performance. In addition, it is strongly desired that the input attributes should be readily derived from data including well logs, a crucial consideration in development of data-driven models involving a vast amount of field data.

On the basis of the sensitivity analysis in chapter 4, it is noted that among numerous parameters influencing SAGD performance (ultimate recovery, remaining trapped bypassed oil, chamber advancement, and heat loss), certain characteristics of the shale barriers (proportions, size, continuity, and position in relation to the well pair) and of lean zones (thickness, oil saturation, and position in relation to the well pair) play a particularly crucial role. The observation that recovery becomes less efficient if the distance between the shale barrier and the well pair decreases, or if the volume or size (length and thickness) of the shale barrier increases, motivates the formulation of a shale indicator $SI = V/d$ (Amirian et al. 2013), where V and d refer to the volume and closest direct distance between a shale barrier and the producer, respectively. In this study, the SI formulation is modified to be a dimensionless quantity: $V/(dwH)$, where w is the reservoir width. In this formulation, $V = L_{sh}H_{sh}W_{sh}$, where L_{sh} , H_{sh} and W_{sh} refer to the length, height and width of the shale barrier, respectively; the product dwH can be considered as the volume of rock between the vertical plane at the heel of the well pair to the corresponding shale barrier. This ratio essentially represents the ratio of shale barrier volume and rock volume between well pair and shale barrier. A vertically continuous shale barrier close to the well pair can be reflected by a high SI value. A similar dimensionless lean-zone indicator can be defined: $LI = V'/(d'wH)$, where V' and d' refer to the volume and closest direct distance between a particular lean zone and the producer. A high LI value describes a thick lean zone very close to the producer. LIT and LIB denote the LI indicator for top water and bottom water, respectively.

A data set consisting of a total of 120 cases with randomly-distributed 1m-thick shale barriers and lean zones with varying thickness and oil content is assembled from the sensitivity-analysis study. One should note that although various aspects of heterogeneities were studied in the past, this study presents an analysis that combines all these effects into a single comprehensive dataset. One can summarize variability among these 120 cases as follows: (1) top-water thickness is between 0 and 100 m ($h_{Dwt} = 0$ to 3.333) (a zero value refers to the absence of lean zone); bottom water thickness is between 0 and 300m ($h_{Dwb} = 0$ to 10); (2) oil saturation in the lean zones is between 0 and 0.95; (3) length of the shale barriers is between 3 and 30m ($l_{Dsh} = 0.06$ to 0.59); and (4) total number of shale barriers is between 2 and 15 (equivalent to 0 to 15% probability of shale occurrence). The total data set (m) is partitioned into two parts: (1) m_1 samples are designated for training and validation of the BPNN model; an n-fold cross validation is implemented to identify the optimal network architecture (Ma et al. 2015); and (2) the remaining $m_2 = m - m_1$ samples are assigned for final testing in a prediction mode with the previously trained network parameters. In this study, the entire data set is subdivided into 70 cases for training, 20 cases for validating, and the remaining 30 cases for testing.

An implementation of ANN modeling in Matlab (R2010b) is used to assess the nonlinear relationships between various pertinent system parameters identified from the sensitivity analysis and SAGD performance indicators (R and DB). Although the influences of heterogeneities were presented in previous studies, formulation of dimensionless variables descriptive of their impacts on SAGD production indicator (or

ranking) are only referred to, but not explicitly defined. A total of 9 dimensionless input variables including SI_{close} , $\langle SI \rangle$, $Var(SI)$, shale proportions, l_{Dsh} , LIT, oil saturation of top water, LIB, and oil saturation of bottom water are adopted in this work. SI_{close} refers to the SI of the shale barrier that is a shortest direct distance to the production well. $\langle SI \rangle$ and $Var(SI)$ refer to the mean and variance of the SI histogram, respectively. Shale proportions are defined as the volume ratio of shale to clean sand and LQS. The data ranges for these 9 variables are tabulated in **Table 5-1**. ANN modeling is repeated with either R or DB designated as the single output.

Although the primary aim of this work is to demonstrate the feasibility of ANN modeling in correlating SAGD performance and to formulate a set of pertinent input attributes that are readily extracted from petrophysical measurements (e.g., logs), it is worthwhile to point out that the selected ranges are comparable with previous studies. The experimental set-up in Yang and Butler (1992) is equivalent to $l_{Dsh} = 0.5$ to 1.0 and a shale thickness of 2m at field scale. Dang et al. (2010) also selected a shale thickness of 1m. Chen et al. (2008) tested a number of stochastic models of shaly sands with correlation length of 1.5m to 24m ($l_{Dsh} = 0.03$ to 0.5) and shale proportions of 10-50%. Pooladi-Darvish and Mattar (2002) modeled a water layer of 2m in the UTF project, but the range in this training dataset encompasses both confined and un- or semi- confined lean zones.

Cross-plots between actual target values and the network predictions for the training data sets are shown in **Fig.5-1 (left) and Fig.5-2 (left)**. Good agreement is observed

between the target values and the ANN predictions. Result of the testing data set (which were not presented to the network previously) are shown in Fig. 5-1 (right) and Fig.5-2 (right), and it can be concluded that trained ANN model yields reasonable predictions for the testing data set. A key conclusion from the ANN modeling results is that the nine proposed input attributes (previously demonstrated to be highly correlated to recovery performance and ranking results) can be used successfully for capturing the effects of heterogeneities as a result of position, continuity, size, proportion of shale barriers, and characteristics (position, thickness, and oil content) of lean zones.

The implementation of SI was tested recently with an SAGD field data set compiled from numerous publicly available sources (Ma et al. 2015). In addition to the typical petrophysical variables including porosity, net-to-gross ratio, saturation and gross pay, it was concluded that the dimensionless SI, which is defined from logs as the shale-barrier thickness divided by distance to well pair, is pertinent in describing the characteristics associated with reservoir heterogeneities and facilitating SAGD-production-performance prediction. The remaining dimensionless attributes adopted in this work, including LI, saturation and shale proportions, can also be derived from log measurements in an analogous fashion.

5.2 Stochastic Distribution of Shale Barrier and Lean Zone

In the section 5.1, good results of ANN modeling demonstrated that these attributes, which can be defined readily from well logs, are highly correlated with the ensuing

recovery response and heat loss. The work also demonstrated the feasibility and utility of data-driven models in correlating SAGD performance.

However, the reservoir heterogeneity modeling in section 5.1 is not realistic such as: (1) the shape of shale/LQS is inerratic; (2) the shale/LQS always distributes in horizontal direction; (3) the size of LQS is limited to be one gridblock surrounding shale barrier; (4) the lean zone distribution within reservoir is not considered; (5) the property of each facie, such as porosity and permeability, are fixed. In this section, the distribution of shale barriers and lean zones will be modeled stochastically as described in chapter 3, and then identify, formulate and correlate a set of attributes pertinent to characterizing stochastic distribution of shale barriers/LQS and lean zones to production performance measures.

Although it is concluded in Chapter 4 that top/bottom water can result in additional heat loss and higher CSOR, it is necessary to examine the effects of stochastically-distributed lean zones on SAGD performance. Two cases are compared: (1) lean zones are distributed stochastically and modeled by the Archie equation as described in Chapter 3 in one case, and (2) constant water saturation that is equal to the mean of the water saturation in the clean sand (0.0667) is assigned. **Fig. 5-3** compares the temperature distributions of the two cases after 10 years simulation. The steam chamber in the reservoir with stochastically-dsitributed lean zone has expanded more quickly. Although a higher RF is observed the corresponding CSOR is also increased; as a result, lower combined R and DB, with higher t_{DISOR} are computed. Therefore, it can be concluded that lean zones can accelerate the expansion of steam chamber by providing additional steam

once they are contacted by the heat. However, the additional heat loss due to higher water thermal conductivity leads to poorer overall efficiency.

The reservoir is assumed to be composed of primarily clean sand, with the combined proportions of shale barriers and LQS to be less than 50%. In particular, LQS proportion is approximately 30% to 50%, whereas the shale barrier proportion is less than 10%, as LQS depicts a gradation of properties between shale barriers and clean sand.

The shale barriers are characterized through proportion, shale range in horizontal direction, shale orientation, and its vertical permeability; the LQS is characterized through proportion, LQS range in horizontal direction, LQS range in vertical direction; and lean zones are characterized through average water saturation of the reservoir. **Fig. 5-4** shows a schematic to illustrate the stochastic heterogeneity-distribution. Here, the correlation lengths of the LQS and shale barriers along the maximum direction of anisotropy (L_{LQS} and L_{sh}) are normalized against the total reservoir length in the x-direction (L): $l_{DLQS} = L_{LQS}/L$ and $l_{Dsh} = L_{sh}/L$, respectively. Similarly, the correlation lengths along the minimum direction of anisotropy (H_{LQS} and H_{sh}) are normalized against the total reservoir thickness (H): $h_{DLQS} = H_{LQS}/H$, and $h_{Dsh} = H_{sh}/H$. Since the physical thickness of a shale barrier is generally smaller than the resolution of the numerical model, H_{sh} is assumed to be a constant value of 1m (size of one grid block); as a result, h_{Dsh} is also a constant. The azimuth angle θ , is measured anti-clockwise away from the x-direction. The value of θ_{sh} is assumed to be quite small, since the shale barriers are typically limited in vertical extent. In addition, θ_{LQS} in LQS is assumed to be the same as

θ_{sh} (i.e. $\theta_{LQS} = \theta_{sh}$) to ensure that the LQS would exist as a transition facie surrounding the shale barriers. Prior to ANN modeling, these azimuth angles are normalized to dimensionless forms as: $\theta_{DLQS} = \theta_{LQS}/360^\circ$ and $\theta_{Dsh} = \theta_{sh}/360^\circ$. These parameters have sufficiently captured the essential information extracted from the semi-variogram models. Other parameters including average k_v/k_h and average water saturation in reservoir $\overline{S_w}$ are computed. All these variables are considered as input attributes for the subsequent ANN modeling, and their ranges are summarized in **Table 5-2**.

In this study, a data set consisting of a total of 50 cases with stochastically-distributed facies, rock properties and lean zones is assembled for ANN modeling, the entire data set is subdivided into 45 cases for training and validating, with the remaining 5 cases for testing.

ANN modeling is implemented in Matlab (R2010b) to correlate the non-linear relationships between the extracted input attributes and multiple SAGD performance indicators (R, DB and t_{DISOR}). A total of 9 dimensionless input attributes including LQS proportion, l_{DLQS} and h_{DLQS} , shale proportion, l_{Dsh} , θ_{Dsh} , k_v/k_h in clean sand and shale, and $\overline{S_w}$ are adopted in this work.

Cross-plots between actual target values and the network predictions for the training data sets are shown in **Figs. 5-5 through 5-7**. In these figures, the output attributes are normalized between their minimum and maximum values to range between 0 and 1. The predictive quality of the ANN models is quantified by the correlation coefficient, and the results are presented in **Table 5-3**. Except for t_{DISOR} , good agreement is observed between

target and predicted values. The results for the testing dataset are also shown in **Figs. 5-5 through 5-7**. It is interesting to observe that the t_{DiSOR} prediction results with the testing dataset are better than those based on the training dataset. Next, PCA is applied to the original dataset, and the number of input attributes is reduced to 5 principal scores. The results as shown in **Figs. 5-8 through 5-10** and Table 5-3 confirm that the removal of internal data redundancy is often needed to improve accuracy and robustness of data-driven models.

Results of Figs. 5-5 through 5-10 seem to suggest that the prediction accuracy for t_{DiSOR} is inferior compared to that for R and DB. It should be noted that t_{iSOR} or iSOR are typically highly sensitive to the specific positions of lean zones in relation to the well pair (Xu et al. 2014a). For instance, significant variation in t_{iSOR} would be expected for two identical reservoirs with the same overall average water saturation, if the lean zones are distributed differently with respect to the well pair.

Finally, only information along the vertical direction of wellbore is extracted to calculate the nine input attributes. This procedure aims to replicate a practical field data set consisting of petrophysical logs available only at vertical delineation wells (Ma et al. 2015). It is obvious that the extracted input variables would capture only a portion of the information related to the reservoir heterogeneity. The objectives of this analysis are to: (1) assess the performance of ANN models when only limited petrophysical information is available; and to (2) illustrate the potential implications of ignoring inter-well heterogeneities. A total of 45 cases are designated for training, and the remaining 5 cases

are employed for testing. The ANN modeling results are shown in **Figs. 5-11, 5-12 and 5-13**. The correlation coefficients are lower than 0.5, a drastic reduction in prediction accuracy comparing to the ANN models constructed in previous section. An improvement is observed between the target values and the ANN predictions when PCA is implemented (**Figs. 5-14, 5-15 and 5-16**). This, again, confirms that the accuracy and robustness of data-driven models can be improved by removing the internal data redundancy.

5.3 Derivation and Calculation of Reservoir Heterogeneities Parameters

In the preceding section, a set of parameters are identified to characterize the reservoir heterogeneities by shale barriers and lean zones. In this section, the method for deriving and calculating these parameters from practical field data is discussed.

Djebbar and Donaldson (2004) presented that it is easy to obtain thickness, water saturation and porosity from well logs, compensated neutron log, density log, sonic log and other methods. The volume and porosity of shale can also be obtained from the well logs (Malureanu et al. 2010). Based on the relation of Wyllie and Rose (1950), a few empirically relations for evaluating the permeability which use porosity and irreducible water saturation. The most well-known relations are Tixier model, Timur model, Coates-Dumanoir model, and Coates model (Schlumberger Ltd., 1989). Hubbard et al. (2011) distinguish facies based on their property difference; therefore it is easy to distinguish LQS from clean sand and shale so that the volume of LQS can be calculated

from the well log data.

Table 5-1 Range of Dimensionless Input Attributes for ANN Modeling

Variable	Min	Max
SI_{close}	0.0006	0.0227
<SI>	0.0059	0.0581
Var(SI)	0.0002	0.3181
Shale Proportions	0.0144	0.1288
I_{Dsh}	0.0275	0.4657
S_o in Bottom Water	0.0000	0.9500
<LIB>	0.0000	2.5000
S_o in Top Water	0.0000	0.9500
<LIT>	0.0000	0.4000

Table 5-2 Range of Dimensionless Input Attributes for ANN Modeling (Stochastic)

Variable	Min	Max
LQS Proportion	0.30	0.50
I_{DLQS}	0.29	0.39
h_{DLQS}	0.17	0.33
Shale Proportion	0.04	0.08
I_{Dsh}	0.17	0.33
θ_{Dsh}	0.00	0.08
k_v/k_h in Clean Sand	0.20	0.80
k_v/k_h in Shale	1.00E-08	1.00E-04
\bar{S}_w	0.11	0.36

Table 5-3 Correlation Coefficients for ANN Modeling (Stochastic)

Output attributes	Base scenario				Ignoring lateral heterogeneity			
	Original 9 input attributes		5 Principal scores		Original 9 input attributes		5 Principal scores	
	Training	Testing	Training	Testing	Training	Testing	Training	Testing
R	0.91	0.72	0.92	0.92	0.46	0.28	0.64	0.92
DB	0.91	0.79	0.91	0.84	0.47	0.39	0.59	0.84
t_{DISOR}	0.48	0.74	0.60	0.79	0.35	0.17	0.59	0.79

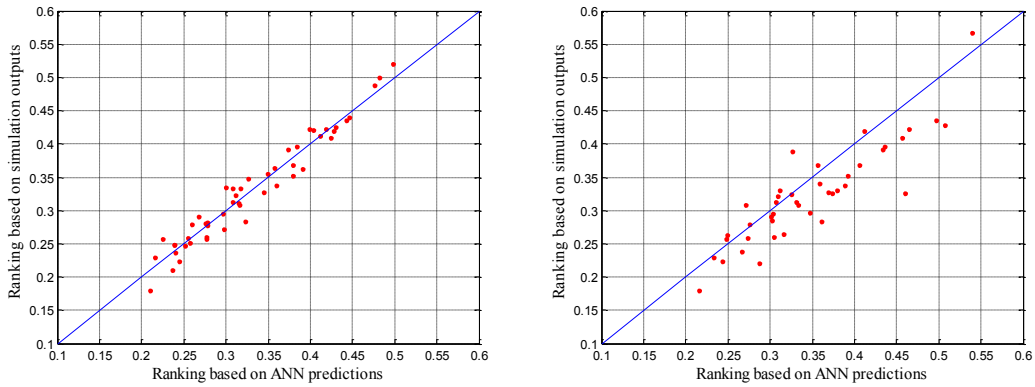


Figure 5-1 Cross plot of actual flow simulation results (target values) of normalized R against network predictions: training data set (left) and testing data set (right).

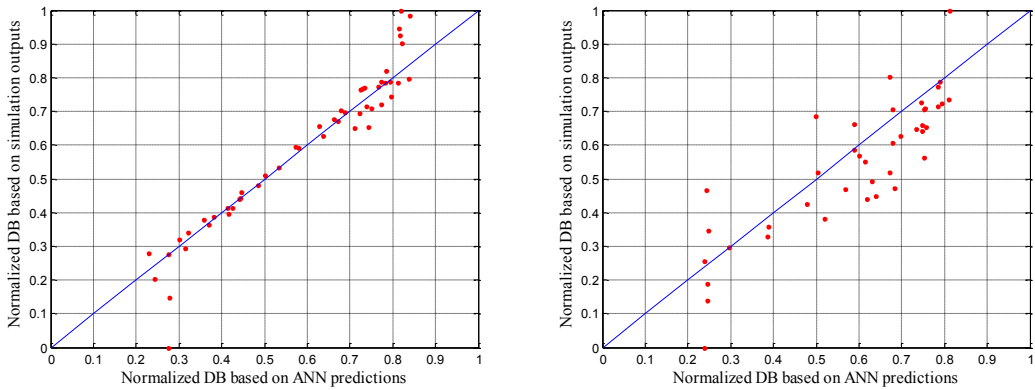


Figure 5-2 Cross plot of actual flow simulation results (target values) of normalized DB against network predictions: training data set (left) and testing data set (right).

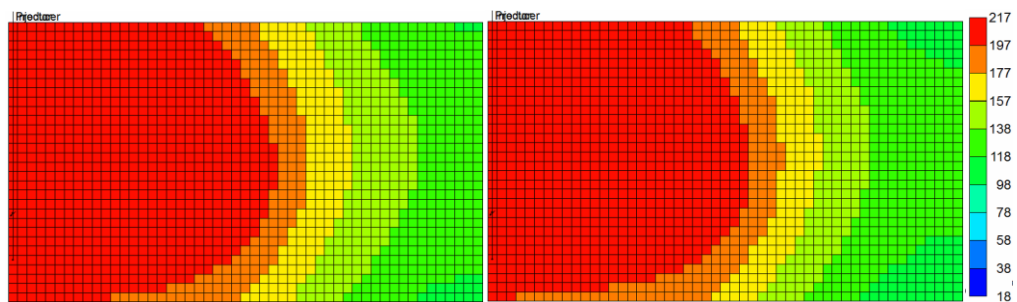


Figure 5-3 Temperature distribution after 10 years SAGD simulation for: Left: stochastic lean zone, and Right: constant water saturation of 0.0667.

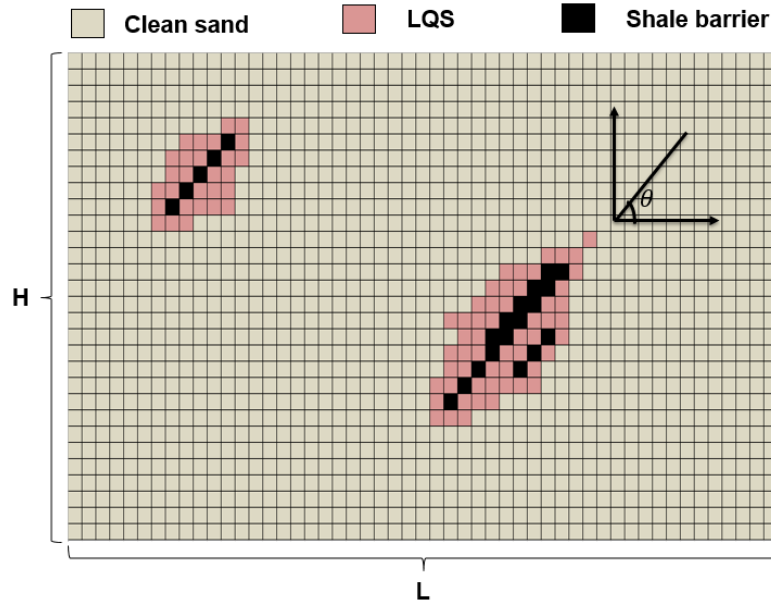


Figure 5-4 Schematic illustrating the stochastic distribution of shale and LQS.

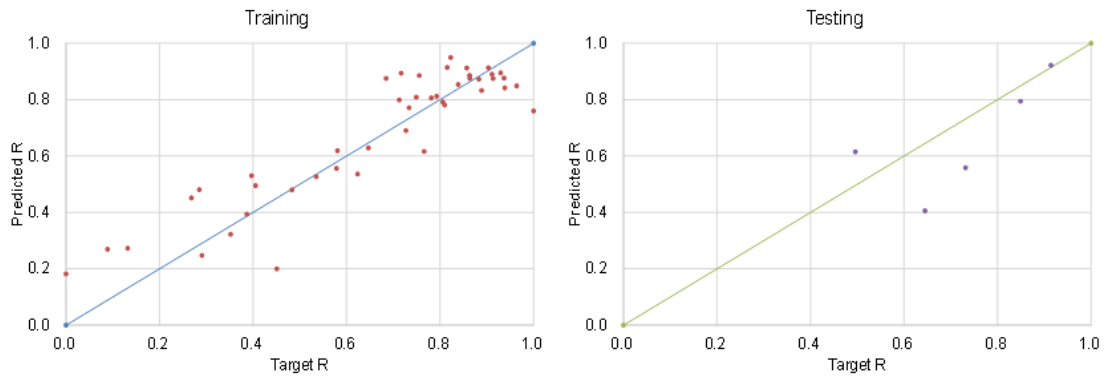


Figure 5-5 Cross plot of actual flow simulation results (target values) of normalized R against network predictions using all 9 original input attributes: training data set (left) and testing data set (right).

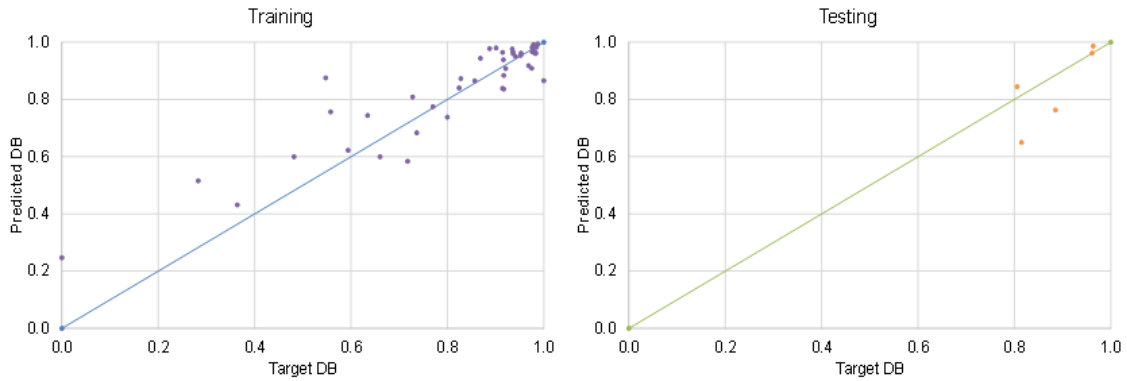


Figure 5-6 Cross plot of actual flow simulation results (target values) of normalized DB against network predictions using all 9 original input attributes: training data set (left) and testing data set (right).

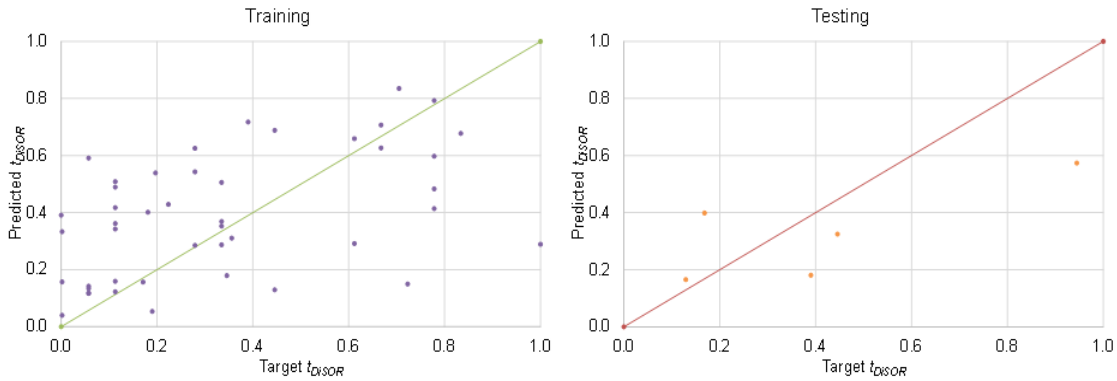


Figure 5-7 Cross plot of actual flow simulation results (target values) of normalized t_{DISOR} against network predictions using all 9 original input attributes: training data set (left) and testing data set (right).

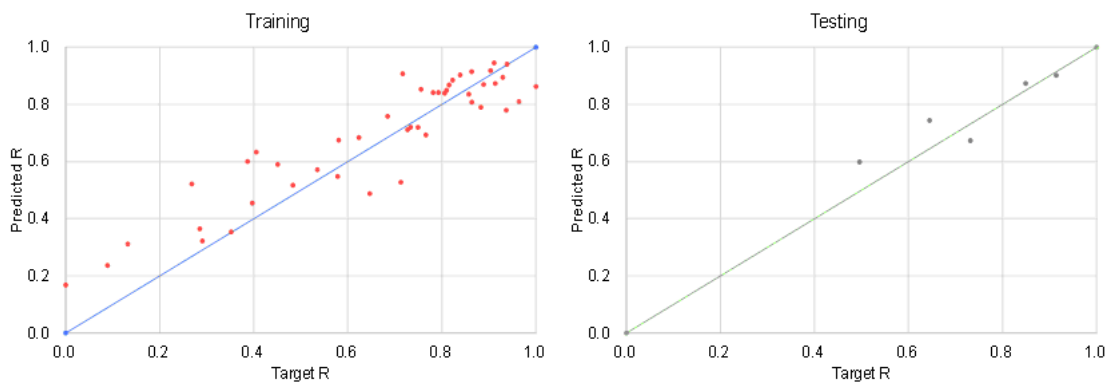


Figure 5-8 Cross plot of actual flow simulation results (target values) of normalized R against network predictions using 5 principal scores as input attributes: training data set (left) and testing data set (right).

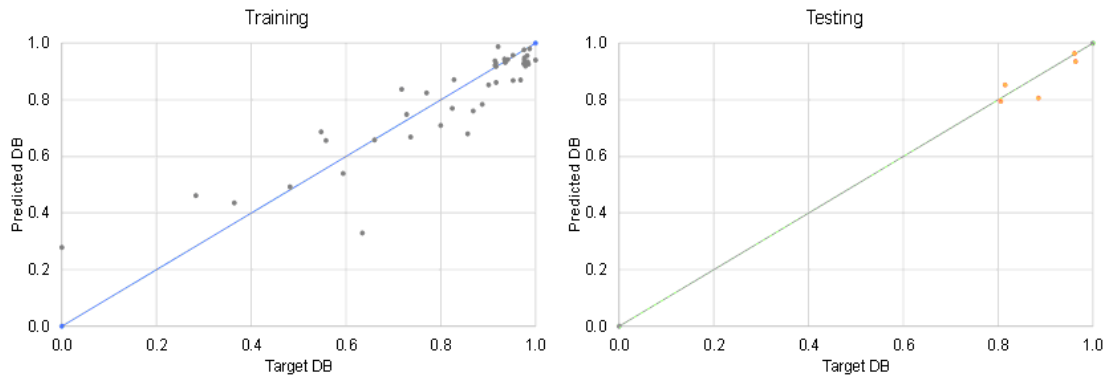


Figure 5-9 Cross plot of actual flow simulation results (target values) of normalized DB against network predictions using 5 principal scores as input attributes: training data set (left) and testing data set (right).

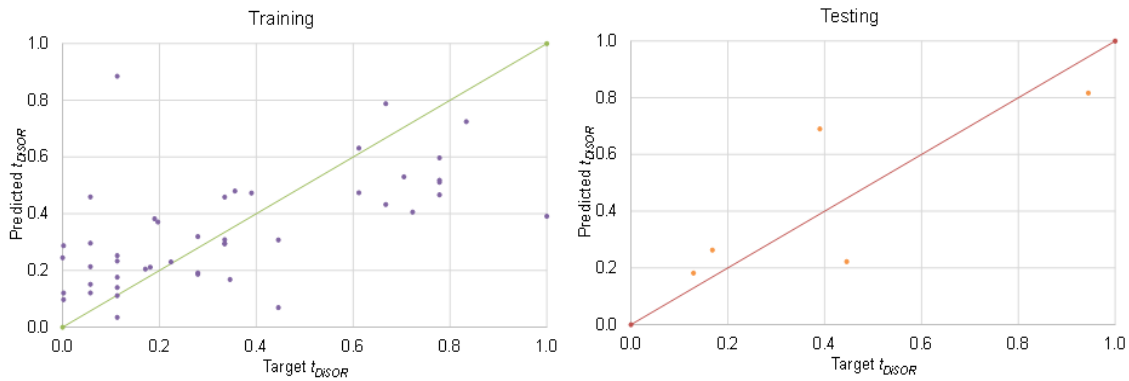


Figure 5-10 Cross plot of actual flow simulation results (target values) of normalized t_{DISOR} against network predictions using 5 principal scores as input attributes: training data set (left) and testing data set (right).

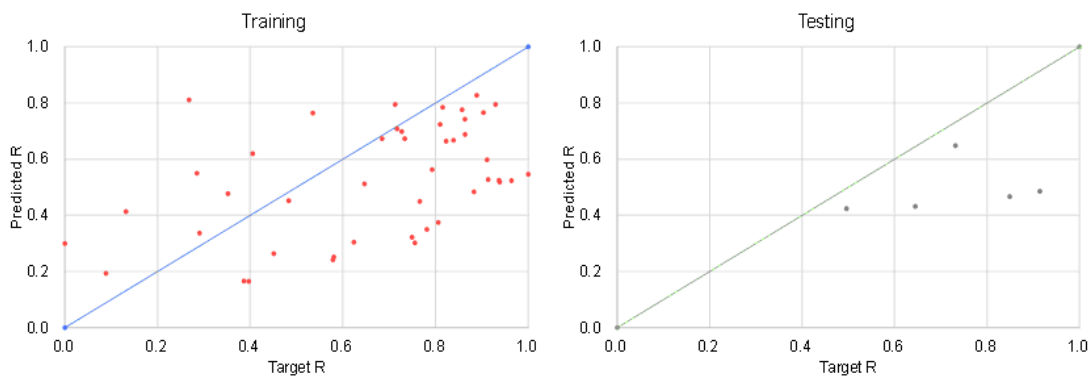


Figure 5-11 Cross plot of actual flow simulation results (target values) of normalized R against network predictions for the case in which lateral heterogeneities are ignored and all 9 original input attributes are used: training data set (left) and testing data set (right).

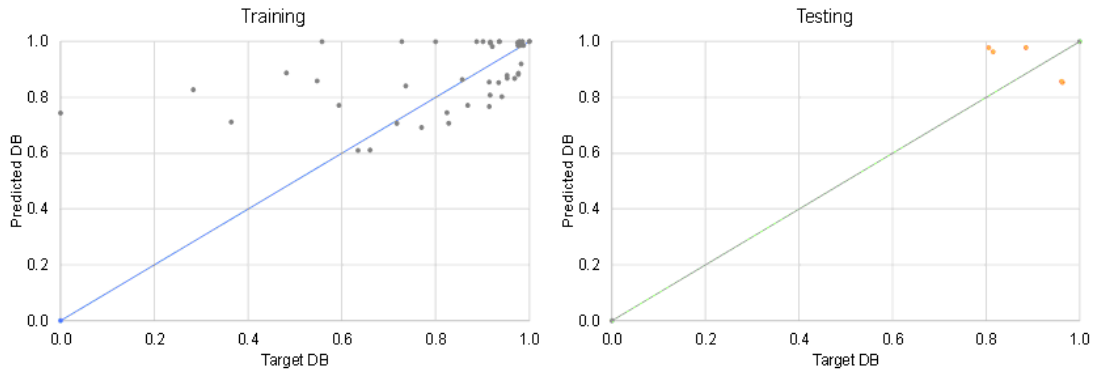


Figure 5-12 Cross plot of actual flow simulation results (target values) of normalized DB against network predictions for the case in which lateral heterogeneities are ignored and all 9 original input attributes are used: training data set (left) and testing data set (right).

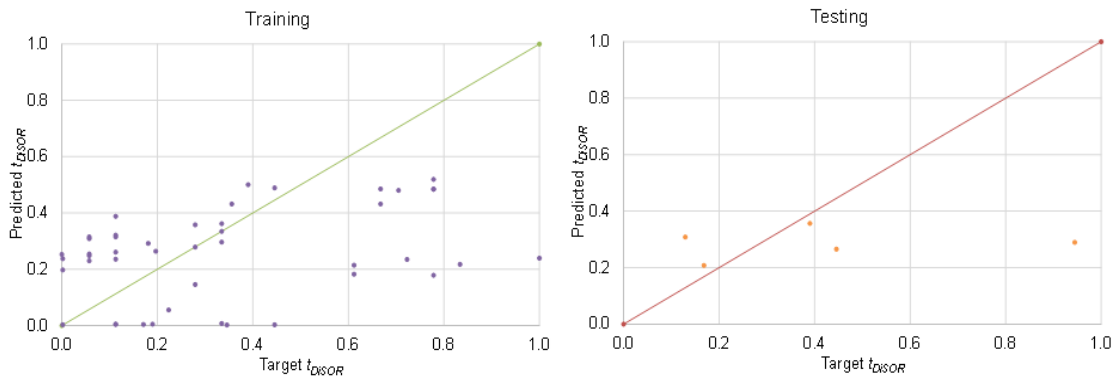


Figure 5-13 Cross plot of actual flow simulation results (target values) of normalized t_{DISOR} against network predictions for the case in which lateral heterogeneities are ignored and all 9 original input attributes are used: training data set (left) and testing data set (right).

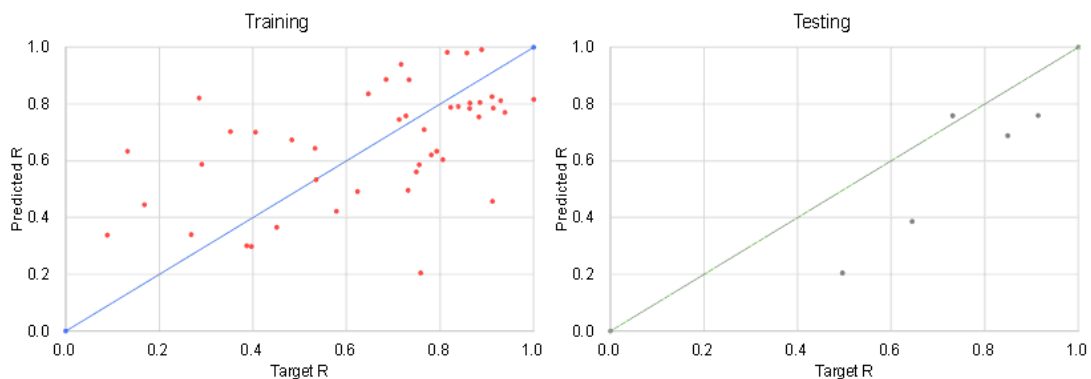


Figure 5-14 Cross plot of actual flow simulation results (target values) of normalized R against network predictions for the case in which lateral heterogeneities are ignored and 5 principal scores are considered as input attributes: training data set (left) and testing data set (right).

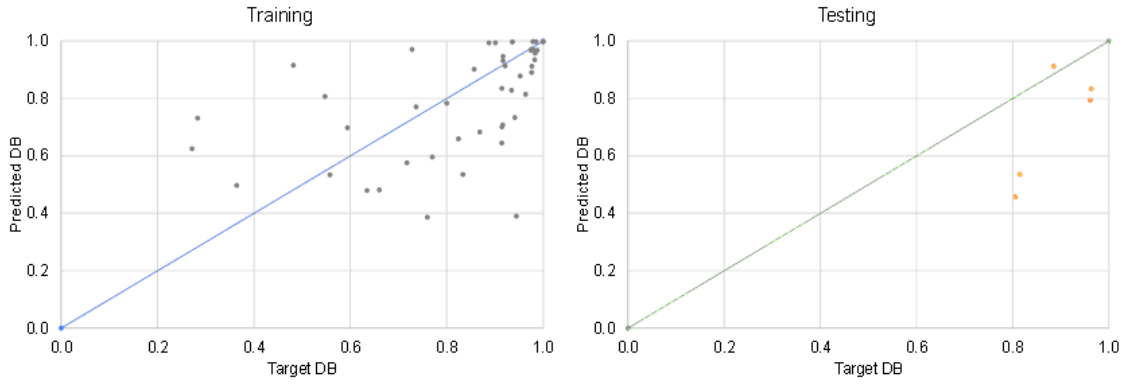


Figure 5-15 Cross plot of actual flow simulation results (target values) of normalized DB against network predictions for the case in which lateral heterogeneities are ignored and 5 principal scores are considered as input attributes: training data set (left) and testing data set (right).

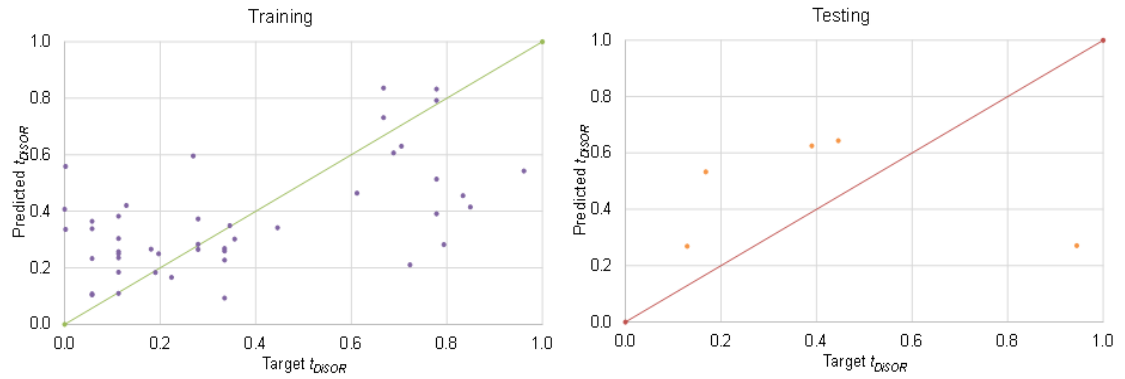


Figure 5-16 Cross plot of actual flow simulation results (target values) of normalized t_{DISOR} against network predictions for the case in which lateral heterogeneities are ignored and 5 principal scores are considered as input attributes: training data set (left) and testing data set (right).

Chapter 6: Conclusion

This thesis has attempted to characterize the effects of reservoir heterogeneities introduced by shale barrier and lean zone on SAGD performance. Their correlation was established using a data-driven model based on the artificial neural networks. A set of parameters that can be directly extracted from well log data are found capable to describe the reservoir heterogeneities and to predict SAGD performance. The research mainly consists of sensitivity analysis for reservoir heterogeneities, modeling of stochastic distribution of shale barrier and lean zone, case study by use of ANN to predict SAGD performance. This chapter summarizes the key points that can be concluded from this research:

1. A comprehensive sensitivity analysis is performed to investigate the effects of heterogeneities in lean zones and shale barriers by varying their location, continuity, size, proportion, and saturation.
 - (1) The results show that heat loss in lean zones would typically result in higher CSOR, despite marginal improvement in RF observed in certain cases. Vaporization from the top water could generate additional steam to accelerate the steam chamber expansion, whereas a lean zone located beneath the producer acts as an energy sink and does not introduce additional benefits of enhancing steam chamber advancement and subsequent oil recovery.
 - (2) Another interesting observation is that although oil saturation in top and bottom water zones does not seem to have a significant impact on SAGD performance in

- this study, they are, nevertheless, important considerations for original oil in place estimation. Thickness of top water is observed to be the dominating factor in controlling CSOR.
- (3) Shale barriers could impeded steam chamber advancement and obstruct oil drainage to the producer. The SAGD performance becomes less efficient if the distance between the shale barrier and the well pair decreases, or if the volume (length and thickness), proportions, or continuity of the shale barrier increases.
2. A main novelty of this simulation study is that shale lenses (imbedded in a region of degraded rock properties referred to as LQS) and lean zones are distributed systematically in reservoir. Capillarity and relative permeability effects, which were ignored in many previous simulation studies, are incorporated in the shale to model bypassed oil trapping.
 3. ANN techniques are applied to construct a data-driven surrogate model to predict SAGD recovery performance. A set of dimensionless input attributes is proposed to capture the heterogeneities of shale barriers and lean zones. Although the influences of heterogeneities were presented in previous studies, the formulation of such dimensionless variables are only referred to, but not explicitly defined. Results of the ANN modeling demonstrate how these input attributes could capture, for instance, the reduction in SAGD performance efficiency with the volume (length and thickness), proportions, or continuity of the shale barrier, or as the distance between the shale barrier and the well pair decreases.

- (1) Nine pertinent dimensionless input attributes including SI_{close} , $\langle SI \rangle$, $Var(SI)$, shale proportions, l_{Dsh} , LIT, LIB, and oil saturation of lean zones are proposed to capture the heterogeneities due to position, continuity, size, proportions of shale barriers, and characteristics (position, thickness, and oil content) of lean zones. Either of the two ranking schemes (R, DB) is taken into account to facilitate the assessment of SAGD performance.
- (2) The formulation of these nine dimensionless input attributes has been extended to represent stochastically distributed shale barriers and lean zones including LQS proportion, l_{DLQS} and h_{DLQS} , shale proportion, l_{Dsh} , θ_{Dsh} , k_v/k_h in clean sand and shale, and $\overline{S_w}$ are proposed to capture the heterogeneities due to proportions, orientation, continuity, saturation, and permeability of different facies. Three production performance indicators (R, DB and t_{DISOR}) that take into account both recovery factor (RF) and cumulative steam injection efficiency (CSOR) are devised to facilitate the assessment of different scenarios. These three indicators capture the main aspects of SAGD efficiency by considering the total oil production, energy consumption associated with steam injection and the overall revenue generation.
- (3) Results of the ANN modeling demonstrate these parameters are capable to describe the reservoir heterogeneities. Common to most data-driven models, removal of internal data redundancy with techniques such as PCA is generally recommended in order to improve model robustness and accuracy.

4. The proposed set of variables can be applied immediately in field-data analysis and scale-up study of experimental models to assist field-operation design and evaluation. This work demonstrated that these attributes, which can be defined readily from well logs, are highly correlated with the SAGD performance (R , DB , t_{DISOR}). A case study is presented to assess the predictability of ANN models when only limited information is available along the vertical direction above a given well pair. The results, though not as good as those where inter-well heterogeneities are accounted for, demonstrate promising potential in the application with practical field data set typically consisting of only petrophysical logs. This work has demonstrated the feasibility and utility of data-driven models in correlating SAGD performance.
5. After this research, formulation of input attributes will include SI and LI when shale barriers sand lean zones are stochastically distributed. Future work should also model the effects of gas cap. In addition, it should incorporate time series data such as the oil rate and instantaneous steam to oil ratio as the ranking criteria.

Nomenclature

Symbols:

a = constant in DB calculation, J/m^3 or cementation factor

a_o = constant, dimensionless

a_w = constant, dimensionless

b = constant in DB calculation, J/m^3

B = notation of matrix (PCA process)

c_o = constant, dimensionless

c_w = constant, dimensionless

C_w = specific heat for water, $J/kg/^\circ C$

C = notation of matrix (PCA process)

d = distance, m or dimension of dataset (PCA process)

d' = distance, m

$f(Y)$ = activation function

H = reservoir thickness, m

H_{LQS} = thickness of LQS, m

H_{sh} = thickness of shale barrier, m

H_{wb} = bottom water zone thickness, m

H_{wt} = top water zone thickness, m

h_{DLQS} = dimensionless thickness of LQS

h_{Dsh} = dimensionless shale thickness

h_{Dwb} = dimensionless bottom water zone thickness

h_{Dwt} = dimensionless top water zone thickness

k_v/k_h = vertical-to-horizontal permeability ratio

L = reservoir length, m or matrix notation (PCA process)

L_{LQS} = length of LQS, m

L_{sh} = length of shale barrier, m

l_{DLQS} = dimensionless length of LQS

l_{Dsh} = dimensionless shale length

M = number of samples in X

m = cementation factor or number of samples in a dataset

m_w = water mass per m^3

m_1 = number of samples for training and validation

m_2 = number of samples for testing

N_r = number of realization

N_h = number of data pairs separated by the distance h

n = saturation exponent or number of input nodes or dimension of dataset (PCA process)

P_c = capillary pressure, kPa

p = dimension of dataset (PCA process)

Q_o = energy of produced oil per cubic meter, J/m^3

Q_w = energy required to generate one cubic meter of steam, J/m^3

R_t = true or formation resistivity, $\Omega \cdot m$

R_w = water resistivity, $\Omega \cdot m$

S_o = oil saturation

S_{or} = residual oil saturation

S_w = water saturation

S_{wr} = residual water saturation

$\overline{S_w}$ = average water saturation in reservoir

t_{iSOR} = duration over which the monthly average steam-to-oil ratio exceeds a threshold,
day

t_{DiSOR} = dimensionless form of t_{iSOR}

t_s = simulation time, year

T_s = surface temperature, $^{\circ}C$

V = shale volume, m^3

V' = lean zone volume, m^3

V_w = vaporization heat for water, kJ/kg

w = width of the reservoir, m

w_0 = bias

w_{ij} = weight associated with the connection between nodes i and j

W_{sh} = width of the shale barrier, m

x = coordinate in horizontal direction

x_i = signal from input node i

y = coordinate in horizontal direction

Y_j = weighted sum of input signals

z = coordinate in vertical direction

ρ_o = oil density, kg/m³

γ = semivariance

ϕ = facy property or porosity

θ = orientation, °

θ_{LQS} = orientation of LQS, °

θ_{sh} = orientation of shale barrier, °

θ_{DLQS} = dimensionless orientation of LQS

θ_{Dsh} = dimensionless orientation of shale barrier

Acronyms:

AIR = above injector region

ANN = artificial neural network

AWR = above well region

BIP = between injector and producer

BPNN = back propagation neural network

CMG = computer modeling group

COP = cumulative oil production

CSS = cyclic steam stimulation

CSOR = cumulative steam oil ratio

DB = discounted barrel

iSOR = monthly average steam-to-oil ratio

LQS = low quality sand

LI = lean zone indicator

LIT = lean zone indicator for top water

LIB = lean zone indicator for bottom water

NWR = near well region

OOIP = original oil in place

PC = principal component

PCA = principal component analysis

PS = principal score

R = ranking indicator

RF = recovery factor

SAGD = steam-assisted gravity drainage

SGSIM = sequential Gaussian simulation

SISIM = sequential indicator simulation

SI = shale indicator

UPR = underneath producer region

UTF = underground test facility

X = original data vector

Z = mean-adjusted data vector

References

- A. Azad and R.J. Chalaturnyk. **2010**. *A Mathematical Improvement to SAGD using Geomechanical Modeling*. Journal of Canadian Petroleum Technology, 49(10), 53-64.
- A.M. Albahlani and T. Babadagli. **2008**. *A Critical Review of the Status of SAGD: Where Are We and What is Next?* SPE Western Regional and Pacific Section AAPG Joint Meeting, Bakersfield, California, USA, 29 March-4 April, SPE 113283.
- C. Bishop. **1995**. *Neural Networks for Pattern Recognition*. Oxford: Clarendon Press.
- C. Bravo, L. Saputelli, F. Rivas, A.G. Perez, M. Nikolaou, and G. Zangl. **2012**. *State-of-the-art Application of Artificial Intelligence and Trends in the E&P Industry: A Technology Survey*. Utrecht, the Netherlands: SPE Intelligent Energy International, March 27-29.
- C. Leskiw and L.D. Gates. **2012**. *Monitoring of SAGD Steam-Chamber Conformance by Using White-Noise-Reflection Processes*. SPE J. 17(04), 1246-1254. SPE 137750.
- Computer Modeling Group. **2013**. *STARS: Advanced Processes & Thermal Reservoir Simulator User's Guide (Version 2013)*. Computer Modeling Group Limited, Calgary, Alberta, Canada.
- C.T.Q. Dang, N.T.B. Nguyen, W. Bae, H.X. Nguyen, T.N. Tu, and T. Chung. **2010**. *Investigation of SAGD Recovery Process in Complex Reservoir*. SPE Asia Pacific Oil & Gas Conference and Exhibition held in Brisbane, Queensland, Australia, 18-20 October, SPE 133849.
- C.V. Deutsch. **2002**. *Geostatistics Reservoir Modeling*. Oxford, UK: Oxford University

Press.

C.V. Deutsch and A.G. Journel. **1998**. *GSLIB. Geostatistical Software Library and User's Guide*. 2nd ed. x + 369 pp. + CD-ROM.

C. Wang and J.Y. Leung. **2015**. *Characterizing the Effects of Lean Zones and Shale Distribution in Steam-Assisted-Gravity-Drainage Recovery Performance*. SPE Reservoir Evaluation & Engineering, 18(03). SPE-170101-PA.

D.D. McCoy, and W.A. Grieves. **1997**. *Use of Resistivity Logs to Calculate Water Saturation at Prudhoe Bay*. SPE-28578-PA.

D.E. Towson. **1977**. *Importance of Reservoir Description in Evaluating In Situ Recovery Methods for Cold Lake Heavy Oil – Part II: In Situ Application*. J.Can.Pet.Tech. Jan.-Mar.

D.G. Smith, S.M. Hubbard, D.A. Leckie, and M. Fustic. **2009**. *Counter Point Bar Deposits: Lithofacies and Reservoir Significance in the Meandering Modern Peace River and Ancient McMurray Formation, Alberta, Canada*. International Association of Sedimentology, 56, 1655-1669.

D.H.-S. Law, T.N. Nasr, and W.K. Goog. **2003**. *Field-Scale Numerical Simulation of SAGD Process With Top-Water Thief Zone*. Journal of Canadian Petroleum Technology, 42(08), 32-38.

E. Amirian, J.Y. Leung, S. Zanon, and P. Dzurman. **2013**. *Data-Driven Modeling Approach for Recovery Performance Prediction in SAGD Operations*. SPE Heavy Oil Conference, Calgary, Alberta, Canada, 11-13 June, SPE 165557.

- E.D. Attanasi and R.F. Meyer. **2007**. *Natural Bitumen and Extra-heavy Oil*. In 2007 Survey of Energy Resources, eds., J. Trinnaman and A. Clarke: World Energy Council, 119-143.
- F. Ahmadloo, K. Asghari, and G. Renouf. **2010**. *A New Diagnostic Tool for Performance Evaluation of Heavy Oil Waterfloods: Case Study of Western Canadian Heavy Oil Reservoirs*. SPE Western Regional Meeting, May 27-29.
- G.E. Archie. **1942**. *The Electrical Resistivity Log as an Aid in Determining Some Reservoir Characteristics*. SPE-942054-G.
- G.H. Kendall. **1977**. *Importance of Reservoir Description in Evaluating In Situ Recovery Methods for Cold Lake Heavy Oil – Part I: Reservoir Description*. J.Can.Pet.Tech. Jan-Mar.
- G. Ipek., T. Frauenfeld, and J.Y. Yuan. **2008**. *Numerical Study of Shale Issues in SAGD*. Canadian International Petroleum Conference, Calgary, Alberta, 17-19 June.
- G.J. Palacky. **1987**. *Clay Mapping using Electromagnetic Methods*. First Break, 5(8), 295-306.
- G. Yang and R.M. Butler. **1992**. *Effects of Reservoir Heterogeneities on Heavy Oil Recovery by Steam-Assisted Gravity Drainage*. Journal of Canadian Petroleum Technology, 31(08), 37-43.
- H.G. Botset. **1940**, *Flow of Gas-Liquid Mixtures Through Consolidated Sand*. Trans., AIM, 136(01), 91-105. SPE-940091-G.
- H.X. Nguyen, W. Bae, V.T. Xuan, Q.T. Dung, and D.H. Nguyen. **2012**. *Effects of*

- Reservoir Parameters and Operational Design on the Prediction of SAGD Performance in Athabasca Oil Sands*. SPE Europec/EAGE Annual Conference, Copenhagen, Denmark, 4-7 June. SPE 154778.
- I.I. Malureanu, V.M. Batistatu, D.-D.M. Neagu. **2010**. *The Analysis of Reservoir Heterogeneity from Well Log Data*. Επιστημονική Επετηρίδα του Τμήματος Γεωλογίας (ΑΠΘ), 99, 149-154.
- J.C. Reis. **1992**. *A Steam-Assisted Gravity Drainage Model for Tar Sands: Linear Geometry*. Journal of Canadian Petroleum Technology, 31(10), 14-20.
- J.F. Goetz, W.J. Prins, J.F. Logar. **1977**. *Reservoir Delineation by Wireline Techniques*. Proceeding Indonesian Petroleum Association Sixth Annual Convention, 161-198.
- J.G. Richardson, D.G. Harris, R.H. Rossen, and G. VanHee. **1978**. *The Effect of Small, Discontinuous Shales on Oil Recovery*. JPT 30(11): 1531-1537. SPE-6700-PA.
- J.T. Morgan and D.T. Gordon. **1970**. *Influence of Pore Geometry on Water-Oil Relative Permeability*. Journal of Petroleum Technology, 22(10), 1199-1208. SPE 2588.
- J. W. P. Vanegas, C. V. Deutsch., and L. B. Cunha. **2008**. *Uncertainty Assessment of SAGD Performance Using a Proxy Model Based on Butler's Theory*. SPE Annual Technical Conference and Exhibition, Denver, Colorado, USA, 21-24 September. SPE 115662.
- J. Wang, M. Dong, and K. Asghari. **2006**. *Effects of Oil Viscosity on Heavy-Oil/Water Relative Permeability Curves*. SPE/DOE Symposium on Improved Oil Recovery, Tulsa, Oklahoma, U.S.A., 22-26 April. SPE 99763.

- J. Zupan. **1994**. *Introduction to Artificial Neural Network (ANN) Methods: What They Are and How to Use Them*. Acta Chimica Slovenica, 41(3), 327-352.
- J.Z. Xu, Z.X. Chen, J.L. Cao, and R. Li. **2014a**. *Numerical Study of the Effects of Lean Zones on SAGD Performance in Periodically Heterogeneous Media*. SPE Heavy Oil Conference held in Alberta, Canada, 2014 June 10-12. SPE-170138-MS.
- J.Z. Xu, Z.X. Chen, Y.G. Yu, and J.L. Cao. **2014b**. *Numerical Thermal Simulation and Optimization of Hybrid CSS/SAGD Process in Long Lake with Lean Zones*. SPE Heavy Oil Conference held in Alberta, Canada, 2014 June 10-12. SPE-170149-MS.
- L. Francis. **2001**. *The Basics of Neural Networks Demystified*. Contingencies, 11(12), 56-61.
- L. Zhao, D.B. Anderson, and C. O'Rourke. **2007**. *Understanding SAGD Producer Wellbore/Reservoir Damage Using Numerical Simulation*. Journal of Canadian Petroleum Technology, 46(01), 50-55.
- MATLAB **2009**. Version 7.9.0 (R2009b). Natick, Massachusetts: The MathWorks Inc.
- M. Ricardo. **2013**. *Simulation Sensitivity Study and Design Parameters Optimization of SAGD Process*. SPE Heavy Oil Conference, Calgary, Alberta, Canada, 11-13 June. SPE 165387.
- M.H. Mohebati, B.B. Maini, and T.G. Harding. **2010**. *Optimization of Hydrocarbon Additives With Steam in SAGD for Three Major Canadian Oil Sands Deposits*. Canadian Unconventional Resources & International Petroleum Conference, Calgary, Alberta, Canada, 19–21 October. CSUG/SPE 138151.

- M, Pooladi-Darvish and L. Mattar. **2002**. *SAGD Operations in the Presence of Overlying Gas Cap and Water Layer – Effect of Shale Layers*. Journal of Canadian Petroleum Technology, 41(06), 40-51.
- M. Shahab. **1995**. *Neural Network: What It Can Do for Petroleum Engineers*. SPE J. 47(01), 42-42. SPE-29219-PA.
- M. Shahab. **2000**. *Virtual-Intelligence Applications in Petroleum Engineering: Part 1 – Artificial Neural Networks*. Journal of Petroleum Technology, 52(09), 64-73. SPE-58046-PA.
- M.R.J. Wyllie and W.D. Rose. **1950**. *Some Theoretical Considerations Related to the Quantitative Evaluation of the Physical Characteristics of Reservoir Rock from Electric Log Data*. Trans, AIME, 189, 105-118.
- N.V. Queipo, J.V. Goicochea, and S. Pintos. **2002**. *Surrogate Modeling-Based Optimization of SAGD Process*. Journal of Petroleum Science and Engineering, 35(1-2): 83-93.
- O.O. Lerat, F. Adjemian, A. Baroni, G. Etienne, G. Renard, E. Bathellier, E. Forgues, F. Aubin, and T. Euzen. **2010**. *Modeling of 4D Seismic Data for the Monitoring of Steam Chamber Growth During the SAGD Process*. Journal of Canadian Petroleum Technology, 49(06), 21-30. SPE 138401.
- Q. Chen. **2009**. *Assessing and Improving Steam-Assisted Gravity Drainage: Reservoir Heterogeneities, Hydraulic Fractures, and Mobility Control*. Dissertation, May, Stanford University.

- Q. Chen, M.G. Gerritsen, and A.R. Kovscek. **2008**. *Effects of Reservoir Heterogeneities on the Steam-Assisted Gravity-Drainage Process*. SPE Reservoir Evaluation & Engineering, 11(05), 921-932. SPE 109873.
- R. Morrow, C.C. Harris. **1965**. *Capillary Equilibrium in Porous Materials*. SPE Journal, 5(1), 15-24. SPE 1011.
- R.C. Burton, L.Y. Chin, E.R. Davis, M. Enderlin, G. Fuh, R. Hodge, G.G. Ramos, P. VanDeVerg, and M. Werner. **2005**. *North Slope Heavy-Oil Sand-Control Strategy: Detailed Case Study of Sand Production Predictions and Field Measurements for Alaskan Heavy-Oil Multilateral Field Developments*. SPE Annual Technical Conference and Exhibition, Dallas, 9-12 October. SPE 97279.
- R.M. Butler. **1985**. *A New Approach To The Modeling Of Steam-Assisted Gravity Drainage*. Journal of Canadian Petroleum Technology, 24(03), 42-51.
- R.M. Butler and G.S. McNab. **1981**. *Theoretical Studies on the Gravity Drainage of Heavy Oil during In-Situ Steam Heating*. Canadian Journal of Chemical Engineering, 59(04), 455-460.
- Schlumberger Ltd. **1989**. *Log Interpretation*. Vol. I-Principles. Houston.
- S. Mohaghegh. **2002**. *Virtual-Intelligence Applications in Petroleum Engineering: Part I Artificial Neural Networks*. Journal of Petroleum Technology, 52(9), 64-73.
- S.D. Joshi, and C.B. Threlkeld. **1985**. *Laboratory Studies of Thermally Aided Gravity Drainage Using Horizontal Wells*. ASOTRA J. Research 2(1): 11.
- S.M. Al-Fattah and R.A. Startzman. **2001**. *Predicting Natural-Gas Production Using*

- Artificial Neural Network*. Paper presented at the 2001 SPE Hydrocarbon Economics and Evaluation Symposium, Dallas, 2-3 April. SPE-68593-MS.
- S.M. Farouq Ali. **1983**. *Effect of Bottom Water and Gas Cap on Thermal Recovery*. SPE Annual California Regional Meeting, Dallas, Texas, March 23-25. SPE 11732.
- S.M. Hubbard, D.G. Smith, H. Nielsen, D.A. Leckie, M. Fustic, R.J. Spencer, and L. Bloom. **2011**. *Seismic Geomorphology and Sedimentology of a Tidally Influenced River Deposit, Lower Cretaceous Athabasca Oil Sands, Alberta, Canada*. The American Association of Petroleum Geologists, 95(07), 1123-1145.
- S.M. Skjaeveland, L.M. Siqveland, A. Kjosavik, W.L. Hammervold Thomas, G.A. Virnovsky. **2000**. *Capillary Pressure Correlation for Mixed-Wet Reservoirs*. SPE Reservoir Eval. & Eng, 3(1), 60-67. SPE 60900.
- S. Masih, K. Ma, J. Sanchez, F. Patino, and L. Boida. **2012**. *The Effect of Bottom Water Coning and Its Monitoring for Optimization in SAGD*. SPE Heavy Oil Conference, Calgary, Alberta, Canada, 12-14 June. SPE 157797.
- T. Djebbar and E.C. Donaldson. **2004**. *Petrophysics-Theory and Practice of Measuring Reservoir Rock and Fluid Transport Properties*. Amsterdam: Elsevier Scientific Publishing Co.
- T. Hampton, D. Kumar, P. Azom, and S. Srinivasan. **2013**. *Analysis of Impact of Thermal and Permeability Heterogeneity on SAGD Performance Using a Semi-Analytical Approach*. SPE Heavy Oil Conference, Calgary, Alberta, Canada, 11-13 June. SPE165565.

- T.N. Nasr, D.H.S. Law, G. Beaulieu, H. Golbeck, G. Korpany, and W.K. Good. **2000**. *SAGD Application in Gas Cap and Top Water Oil Reservoirs*. Canadian International Petroleum Conference, 4-8 June, Calgary, Alberta.
- T.N. Nasr and O.R. Ayodele. **2006**. *New Hybrid Steam-Solvent Process for the Recovery of Heavy Oil and Bitumen*. Abu Dhabi International Petroleum Exhibition and Conference, Abu Dhabi, 5-8 November. SPE 101717.
- W.K. Good, R. Claude, and B. D. Felty. **1997**. *Possible Effects of Gas Caps on SAGD Performance*. ADOE/EUB Report.
- W.S. McCulloch, and W. Pitts. **1943**. *A Logical Calculus of Ideas Immanent in Nervous Activity*. Bulletin of Mathematical Biophysics. 5, 115-133.
- W.W. Weiss, R.S. Balch, and B.A. Stubbs. **2002**. *How Artificial Intelligence Methods Can Forecast Oil Production*. Paper presented at the 2002 SPE/DOE Improved Oil Recovery Symposium, Tulsa, 13-17 April. SPE-75143-MS.
- Y. Iwata, H. Koseki, M.L. Janssens, and T. Takahashi. **2000**. *Comparison of Combustion Characteristics of Various Crude Oils*. International Association for Fire Safety Science AOFST 4.
- Z. Ma, J. Leung, S. Zanon, and P. Dzumann. **2015**. *Practical Implementation of Knowledge-Based Approaches for SAGD Production Analysis*. Expert Systems with Applications, 42(21): 7326-7343.


```

fid_SIclose=fopen(SIclosefilename,'w');
fid_shaleclose=fopen(Shaleclosefilename,'w');
fid_SImean=fopen(SImeanfilename,'w');
fid_SIVariance=fopen(SIVariancefilename,'w');
fid_AL=fopen(Averagelength,'w');
fid_AP=fopen(Averageporosity,'w');
fid_ASW=fopen(AverageSw,'w');
fid_SP=fopen(Shaleproportion,'w');
fid_LQSP=fopen(LQSproportion,'w');
fid_OOIP=fopen(OOIP,'w');
fid_COP=fopen(cumu_oil_pro,'w');
fid_CWI=fopen(cumu_water_inj,'w');
Aporosand=zeros(multiple_num,1);
Aporoshale=zeros(multiple_num,1);
Apermsand=zeros(multiple_num,1);
Apermshale=zeros(multiple_num,1);

% read porosity of shale, LQS, and clean sand
datarange='B4:B1533';
filename='Realization.xlsx';
filename2='Saturation of 3 facies.xlsx';
porosand=xlsread(filename,1,datarange);
porolqs=xlsread(filename,2,datarange);
poroshale=xlsread(filename,3,datarange);
numgrid=length(porosand);
% swsand=xlsread(filename2,1,datarange);
swsand=(0.2*ones(numgrid,1))./(500*ones(numgrid,1))./(porosand).^2).^1/2);

```

```

% swlqs=xlsread(filename2,2,datarange);
swlqs=(0.2*ones(numgrid,1)./(300*ones(numgrid,1))./(porolqs).^2).^(1/2.5);
% swshale=xlsread(filename2,3,datarange);
swshale=(0.2*ones(numgrid,1)./(100*ones(numgrid,1))./(poroshale).^2).^(1/3);
for i=1:length(swsand)
    if swsand(i,1)<0
        swsand(i,1)=0;
    elseif swsand(i,1)>1
        swsand(i,1)=1;
    end
    if swlqs(i,1)<0
        swlqs(i,1)=0;
    elseif swlqs(i,1)>1
        swlqs(i,1)=1;
    end
    if swshale(i,1)<0
        swshale(i,1)=0;
    elseif swshale(i,1)>1
        swshale(i,1)=1;
    end
end
perm=0.5;
kvkhsand=rand(1,multiple_num)*0.6+0.2;
kvkshale=ones(1,multiple_num)*1e-4+1e-8;
kvkhlqs=0.5*(kvkhsand+kvkshale);
permsand=perm*kvkhsand;
permlqs=perm*kvkhlqs;

```

```

permshale=perm*kvkhshale;

for i=1:multiple_num

    % read the facy data for shale, LQS, and clean sand
    facy1name=strcat('sisim',int2str(i),'_1.txt');
    facy2name=strcat('sisim',int2str(i),'_2.txt');
    idfacy1=datread(facy1name);
    idfacy2=datread(facy2name);

    % cui wang at 2015 July 17th
    idfacyplot=ones(30*51,1)*0.9;
    poroplot=porosand;
    swplot=swsand;
    for m=1:30*51
        if idfacy1(m,1)==1
            if idfacy2(m,1)==1
                idfacyplot(m,1)=0.1;
                poroplot(m,1)=poroshale(m,1);
                swplot(m,1)=swshale(m,1);
            else
                idfacyplot(m,1)=0.5;
                poroplot(m,1)=porolqs(m,1);
                swplot(m,1)=swlqs(m,1);
            end
        end
    end
end
end
end

```

```
% cui wang at 2015 July 17th
```

```
idfacym1=reshape(idfacy1,51,30)';
```

```
idfacym2=reshape(idfacy2,51,30)';
```

```
porosandm=reshape(porosand,51,30)';
```

```
porolqsm=reshape(porolqs,51,30)';
```

```
poroshalem=reshape(poroshale,51,30)';
```

```
swsandm=reshape(swsand,51,30)';
```

```
swlqsm=reshape(swlqs,51,30)';
```

```
swshalem=reshape(swshale,51,30)';
```

```
for nr=1:30
```

```
    nrr=31-nr;
```

```
    idfacymnew1(nr,:)=idfacym1(nrr,:);
```

```
    idfacymnew2(nr,:)=idfacym2(nrr,:);
```

```
    porosandmnew(nr,:)=porosandm(nrr,:);
```

```
    porolqsmnew(nr,:)=porolqsm(nrr,:);
```

```
    poroshalemnew(nr,:)=poroshalem(nrr,:);
```

```
    swsandmnew(nr,:)=swsandm(nrr,:);
```

```
    swlqsmnew(nr,:)=swlqsm(nrr,:);
```

```
    swshalemnew(nr,:)=swshalem(nrr,:);
```

```
end
```

```
idfacym1=idfacymnew1;
```

```
idfacym2=idfacymnew2;
```

```
porosandm=porosandmnew;
```

```
porolqsm=porolqsmnew;
```

```
poroshalem=poroshalemnew;  
swsandm=swsandmnew;  
swlqsm=swlqsmnew;  
swshalem=swshalemnew;
```

```
porostring(1,1)=' '  
swstring(1,1)=' '  
sostring(1,1)=' '  
permstring=' '  
permstringv=' '  
permmodel='mod';
```

```
idfacym=ones(30,51)*2;  
for m=1:30  
    for n=1:51  
        if idfacym1(m,n)==1  
            if idfacym2(m,n)==1  
                idfacym(m,n)=0;  
            else  
                idfacym(m,n)=1;  
            end  
        end  
    end  
end  
end
```

```
ns=1; %number of shale
```

```

shalelength=0; %shale length
xshale=0; %shale x coordinate
yshale=0; %shale y coordinate
idnum=0;
idstring=1;

sumsandporo=0;
sumlqsporo=0;
sumsandperm=0;
sumshaleporo=0;
sumshaleperm=0;
sumsandsw=0;
sumlqssw=0;
sumshalesw=0;
numsand=0;
numlqs=0;
numshale=0;
oo=0;

for m=1:30
    for n=1:51
        if idfacym(m,n)==2
            porostring=strcat(porostring,32,num2str(porosandm(m,n)));
            swstring=strcat(swstring,32,num2str(swsandm(m,n)));
            sostring=strcat(sostring,32,num2str(1-swsandm(m,n)));

            permstring=strcat(permstring,32,num2str(perm));

```

```
permstringv=strcat(permstringv,32,num2str(permsand(1,i)));
```

```
sumsandporo=sumsandporo+porosandm(m,n);
```

```
sumsandsw=sumsandsw+porosandm(m,n);
```

```
sumsandperm=sumsandperm+perm;
```

```
numsand=numsand+1;
```

```
oo=oo+1*1*900*porosandm(m,n)*(1-swsandm(m,n));
```

```
elseif idfacym(m,n)==0
```

```
porostring=strcat(porostring,32,num2str(poroshalem(m,n)));
```

```
swstring=strcat(swstring,32,num2str(swshalem(m,n)));
```

```
sostring=strcat(sostring,32,num2str(1-swshalem(m,n)));
```

```
permstring=strcat(permstring,32,num2str(perm));
```

```
permstringv=strcat(permstringv,32,num2str(permshale(1,i)));
```

```
sumshaleporo=sumshaleporo+poroshalem(m,n);
```

```
sumshalesw=sumshalesw+swshalem(m,n);
```

```
sumshaleperm=sumshaleperm+perm;
```

```
numshale=numshale+1;
```

```
oo=oo+1*1*900*poroshalem(m,n)*(1-swshalem(m,n));
```

```
shalelength(ns,1)=shalelength(ns,1)+1;
```

```
if n-1>=1
```

```

        if idfacym(m,n-1)~=0
            xshale(ns,1)=n;
            yshale(ns,1)=m;
        end
    end
    if n==1 & idfacym(m,n)==0
        xshale(ns,1)=n;
        yshale(ns,1)=m;
    end

    if n+1<=51
        if idfacym(m,n+1)~=0
            ns=ns+1;
            shalelength(ns,1)=0;
        end
    end
    if n==51 & idfacym(m,n)==0
        ns=ns+1;
        shalelength(ns,1)=0;
    end

else
    porostring=strcat(porostring,32,num2str(poroIQsm(m,n)));
    swstring=strcat(swstring,32,num2str(swlQsm(m,n)));
    sostring=strcat(sostring,32,num2str(1-swlQsm(m,n)));

    permstring=strcat(permstring,32,num2str(perm));

```

```

        permstringv=strcat(permstringv,32,num2str(permlqs(1,i)));
        sumlqsporo=sumlqsporo+porolqsm(m,n);
        sumlqssw=sumlqssw+swlqsm(m,n);
        numlqs=numlqs+1;
        oo=oo+1*1*900*porolqsm(m,n)*(1-swlqsm(m,n));

    end

end

end

ooip(i,1)=oo;
Aporosand(i,1)=sumsandporo/numsand;
Apermsand(i,1)=sumsandperm/numsand;
Aporoshale(i,1)=sumshaleporo/numshale;
Apermshale(i,1)=sumshaleperm/numshale;
ns=ns-1;
lengthshale=zeros(ns,1);
xshaleend=zeros(ns,1);
SI=zeros(ns,1);
d=zeros(ns,1);

for idshale=1:ns
    lengthshale(idshale,1)=shalelength(idshale,1);
    xshaleend(idshale,1)=xshale(idshale,1)-1+lengthshale(idshale,1);
    d(idshale,1)=sqrt(xshale(idshale,1)^2+(yshale(idshale,1)-26)^2);
    SI(idshale,1)=lengthshale(idshale,1)/d(idshale,1)/51/30;
end

[mind,minp]=min(d);

```

```

Lengthclose=lengthshale(minp);
SIclose=SI(minp);
SImean=sum(SI)/ns;
SIvariance=sum((SI-SImean).^2)/ns;
SP=sum(shalelength)/51/30;
LQSP=numlqs/51/30;
AL=sum(lengthshale)/ns;
AP=(sumsandporo+sumlqsporo+sumshaleporo)/51/30;
ASW=(sumsandsw+sumlqssw+sumshalesw)/51/30;

fprintf(fid_SIclose,[strcat(num2str(SIclose),32) '\n']);
fprintf(fid_shaleclose,[strcat(num2str(Lengthclose),32) '\n']);
fprintf(fid_SImean,[strcat(num2str(SImean),32) '\n']);
fprintf(fid_SIvariance,[strcat(num2str(SIvariance),32) '\n']);
fprintf(fid_AL,[strcat(num2str(AL),32) '\n']);
fprintf(fid_AP,[strcat(num2str(AP),32) '\n']);
fprintf(fid_ASW,[strcat(num2str(ASW),32) '\n']);
fprintf(fid_SP,[strcat(num2str(SP),32) '\n']);
fprintf(fid_LQSP,[strcat(num2str(LQSP),32) '\n']);
fprintf(fid_OOIP,[strcat(num2str(oo),32) '\n']);

newcasename=strcat('basecaseANN',num2str(i),'.dat');
fidr=fopen(basename,'r');
fidw=fopen(newcasename,'w');
frewind(fidr)
a=0;
while ~feof(fidr)

```

```

a=a+1;
lines{a} = fgetl(fidr);
if a==82
    lines{a}=porostring;
end
if a==84
    lines{a}=permstring;
end
if a==87
    lines{a}=permstringv;
end
for idshale=1:ns
    linenum=idshale+273;
    if linenum==274 && a==linenum

lines{a}=strcat('mod',32,int2str(xshale(idshale)),';',int2str(xshaleend(idshale)),32,int2str(
1),':',int2str(1),32,int2str(yshale(idshale)),';',int2str(yshale(idshale)),32,'=',32,int2str(2));
        end
        if linenum>274 && a==linenum

lines{a}=strcat(32,int2str(xshale(idshale)),';',int2str(xshaleend(idshale)),32,int2str(1),':',in
t2str(1),32,int2str(yshale(idshale)),';',int2str(yshale(idshale)),32,'=',32,int2str(2));
        end
    end
    if a==397
        lines{a}=swstring;
    end
end

```

```

    if a==399
        lines{a}=sostring;
    end
    fprintf(fidw,[lines {a}  '\n']);
end

```

```

simulatorPath='C:\Program
Files(x86)\CMG\STARS\2013.10\Win_x64\EXE\st201310.exe';
resultReportPath = 'C:\Program Files (x86)\CMG\BR\2013.10\Win_x64\EXE\report.exe';
workDirectoryPath = 'E:\\Cui\\Cases generation using SISIM porosity lean zones\\';
command=strcat('','simulatorPath',' -f ', newcasename,' -wd ', workDirectoryPath, '
-log ', ' -wait ');
system(command);
newModelName=newcasename;

```

```

    irfFilePath = strrep(newModelName,'.dat','.irf');
    rwdFilePath = strrep(newModelName,'.dat','.rwd');
    % create rwd file
    writeFileID = fopen(rwdFilePath,'w');
        % UPDATE THIS
        fprintf(writeFileID,'*SPREADSHEET ');
        fprintf(writeFileID,'\n');
        fprintf(writeFileID,'*TIME ON ');
        fprintf(writeFileID,'\n');
        fprintf(writeFileID,'*FILES ');
        fprintf(writeFileID,'');
        fprintf(writeFileID,irfFilePath);

```

```

        fprintf(writeFileID, "");
        fprintf(writeFileID, '\n');
        fprintf(writeFileID, '*TABLE-FOR ');
        fprintf(writeFileID, '\n');
        fprintf(writeFileID, ' *COLUMN-FOR *WELL ');
        fprintf(writeFileID, "");
        fprintf(writeFileID, 'Producer');
        fprintf(writeFileID, "");
        fprintf(writeFileID, '\n');
        fprintf(writeFileID, ' *PARAMETERS ');
        fprintf(writeFileID, "");
        fprintf(writeFileID, 'Cumulative Oil SC');
        fprintf(writeFileID, "");
        fprintf(writeFileID, '\n');
        fprintf(writeFileID, '*TABLE-END ');

    fclose(writeFileID);

% create rwo file
rwoFilePath = strrep(newModelName, '.dat', '.rwo');

% execute result report to rwo file
command = strcat("", resultReportPath, " -f ", rwdFilePath, " -o ", rwoFilePath);
system(command);

%
%

% open the rwo file
% read line by line
    foutputfileid = fopen(rwoFilePath); %close this file?
    tline = fgetl(foutputfileid);

```

```

while ~feof(foutputfileid)
    tline = fgetl(foutputfileid);
end

%
%
% create _w.rwd file
rwdFilePath_w = strep(newModelName,'.dat','_w.rwd');
writeFileID_w = fopen(rwdFilePath_w,'w');

%
    UPDATE THIS

    fprintf(writeFileID_w,'*SPREADSHEET ');
    fprintf(writeFileID_w,'\n');
    fprintf(writeFileID_w,'*TIME ON ');
    fprintf(writeFileID_w,'\n');
    fprintf(writeFileID_w,'*FILES ');
    fprintf(writeFileID_w,'');
    fprintf(writeFileID_w,irfFilePath);
    fprintf(writeFileID_w,'');
    fprintf(writeFileID_w,'\n');
    fprintf(writeFileID_w,'*TABLE-FOR ');
    fprintf(writeFileID_w,'\n');
    fprintf(writeFileID_w,' *COLUMN-FOR *WELL ');
    fprintf(writeFileID_w,'');
    fprintf(writeFileID_w,'Injector');
    fprintf(writeFileID_w,'');
    fprintf(writeFileID_w,'\n');
    fprintf(writeFileID_w,' *PARAMETERS ');
    fprintf(writeFileID_w,'');
    fprintf(writeFileID_w,'Cumulative Water SC');

```

```

        fprintf(writeFileID_w,"");
        fprintf(writeFileID_w,'\n');
        fprintf(writeFileID_w,'*TABLE-END ');
    fclose(writeFileID_w);

% create _w.rwo file
rwoFilePath_w = strep(newModelName,'.dat','_w.rwo');

% execute result report to _w.rwo file
command = strcat("",resultReportPath," -f ", rwdFilePath_w," -o ",
rwoFilePath_w);
system(command);

% open the _w.rwo file
% read line by line
    foutputfileid_w = fopen(rwoFilePath_w);
    tline_w = fgetl(foutputfileid_w);
    while ~feof(foutputfileid_w)
        tline = fgetl(foutputfileid_w);
    end

%
% writing the output data to the txt files
    originalModelName = strcat(workDirectoryPath,'basecaseANN1.rwo');
    newModelName=strep(originalModelName,'1.rwo',strcat(int2str(i),'.rwo'));

newModelName_w=strep(originalModelName,'1.rwo',strcat(int2str(i),'_w.rwo'));
    fid=fopen(newModelName, 'r');
    fid_w=fopen(newModelName_w, 'r');

```

```

    frewind(fid);
    while ~feof(fid)
        COP_FINAL= fgetl(fid);
    end
    fprintf(fid_COP,[COP_FINAL '\n']);
    while ~feof(fid_w)
        CWI_FINAL= fgetl(fid_w);
    end
    fprintf(fid_CWI,[CWI_FINAL '\n']);

end

fclose(fidr);
fclose(fidw);
fclose(fid_AL);
fclose(fid_AP);
fclose(fid_Slclose);
fclose(fid_shaleclose);
fclose(fid_SImean);
fclose(fid_Slvariance);
fclose(fid_SP);
fclose(fid_COP);
fclose(fid_CWI);

```

Appendix B: Calculation of DB

The net energy obtained from the entire SAGD process can be expressed mathematically as discounted barrels: $DB \text{ (BTU/bbl)} = Q_o - CSOR \times Q_w$. The quantity of DB is interpreted as the energy of the produced oil at surface conditions (1atm, 15°C), while Q_o

and Q_w refer to the energy content of one barrel of oil and steam, respectively. Q_o is computed from the oil density (ρ_o in kg/m^3) based on the empirical relationship by Iwata et al. (2000): $Q_o = a + b \times \rho_o$, where $a = 4.11 \times 10^{10} \text{ J/m}^3$ and $b = 3.80 \times 10^7 \text{ J/kg}$, while Q_w is estimated to be $m_w \times C_w \times (100 - T_s) + m_w \times V_w$, where m_w refers to the mass of water per barrel (100 kg/m^3); C_w and V_w are the specific heat ($200 \text{ J/kg/}^\circ\text{C}$) and heat of vaporization of water (2260 kJ/kg), respectively; T_s is the surface temperature (15°C).